

## The Cannonball Model of Gamma Ray Bursts: high-energy neutrinos and $\gamma$ -rays

Arnon Dar<sup>a</sup> and A. De Rújula<sup>b</sup>

<sup>a</sup>) Physics Department and Space Research Institute, Technion, Haifa 32000, Israel

<sup>b</sup>) Theory Division, CERN, 1211 Geneva 23, Switzerland

### Abstract

Recent observations suggest that  $\gamma$ -ray bursts (GRBs) and their afterglows are produced by jets of highly relativistic cannonballs (CBs), emitted in supernova (SN) explosions. The CBs, reheated by their collision with the shell, emit radiation that is collimated along their direction of motion and Doppler-boosted to the typical few-hundred keV energy of the GRB. Accompanying the GRB, there should be an intense burst of neutrinos of a few hundreds of GeV energy, made by the decay of charged pions produced in the collisions of the CBs with the SN shell. The neutrino beam carries almost all of the emitted energy, but is much narrower than the GRB beam and should only be detected in coincidence with the small fraction of GRBs whose CBs are moving very close to the line of sight. The neutral pions made in the transparent outskirts of the SN shell decay into energetic  $\gamma$ -rays (EGRs) of energy of  $\mathcal{O}(100)$  GeV. The EGR beam, whose energy fluence is comparable to that of the companion GRB, is as wide as the GRB beam and should be observable, in coincidence with GRBs, with existing or planned detectors. We derive in detail these predictions of the CB model.

# 1 Introduction

For a third of a century, gamma ray bursts (GRBs) have constituted a great astrophysical mystery. Their origin is still an unresolved enigma, in spite of recent remarkable observations in the field: the discovery of GRB afterglows [1, 2], the discovery [3] of the association of GRBs with supernovae (SNe), and the measurements of the redshifts [4] of their host galaxies. The current generally accepted view is that GRBs are generated by synchrotron emission from relativistically expanding fireballs, or firecones, produced by collapses or mergers of compact stars [5], by failed supernovae or collapsars [6], or by hypernova explosions [7]. It was further suggested that these highly relativistic fireballs produce large fluxes of very high energy neutrinos in coincidence with the GRBs [8]. But various observations suggest that most GRBs are produced by highly collimated superluminal jets and not by relativistically expanding fireballs [9, 10, 11, 12].

In a recent series of papers [12, 22, 23] we have outlined a cannonball (CB) model of GRBs which, we contend, is capable of describing the GRB phenomenology, and results in interesting predictions. The CB model is based on the following analogies, hypothesis and explicit calculations:

*Jets in astrophysics.* Astrophysical systems, such as quasars and microquasars, in which periods of intense accretion into a massive object occur, emit highly collimated jets of plasma. The Lorentz factor  $\gamma \equiv 1/\sqrt{1 - v^2/c^2}$  of these jets ranges from mildly relativistic:  $\gamma \sim 2.55$  for PSR 1915+13 [24], to quite relativistic:  $\gamma = \mathcal{O}(10)$  for typical quasars [25], and even to highly relativistic:  $\gamma \sim 10^3$  for PKS 0405–385 [26]. These jets are not continuous streams of matter, but consist of individual blobs, or “cannonballs”. The mechanism producing these surprisingly energetic and collimated emissions is not understood, but it seems to operate pervasively in nature. We assume the CBs to be composed of ordinary “baryonic” matter (as opposed to  $e^+ e^-$  pairs), as is the case in the microquasar SS 433, from which  $\text{Ly}_\alpha$  and metal  $\text{K}_\alpha$  lines have been detected [27, 28].

*The GRB/SN association.* The original observation of a spatial and a temporal coincidence between GRB 980425 and the relatively close-by supernova SN 1998bw (redshift  $z = 0.0085$ ), that suggested a physical association [3], has developed into a much more convincing case for the claim [12] that many, perhaps *all*, of the long-duration GRBs are associated with SNe. Indeed, of the dozen and a half GRBs whose redshift is known, the nearest six that have redshifts  $z < 1$  show in their afterglow an additive “bump”, with the time dependence and spectrum of a SN akin to 1998bw properly corrected [12], [13] for the different redshift values and galactic extinction [13]: GRB 990228 [14], [15], [16]; GRB 970508 [17]; GRB 980703 [18]; GRB 990712 [19], [20]; GRB 991208 [21]; GRB 000418 [12].

In all the other cases with larger redshifts there is one or more good reasons for

such a bump not to have been seen: no observations of the afterglow at late time are available, the expected bump is below the sensitivity of the late time observations, the spectrum of SN 1998bw is not known at the frequencies required to extrapolate its light curve to a much higher  $z$ . Thus, observationally, seven out of sixteen —and perhaps all— of the GRBs of known redshift have a SN associated with them. The energy supply in a SN event similar to SN 1998bw is too small to accommodate the fluence of cosmological GRBs, unless their  $\gamma$ -rays are highly beamed. SN 1998bw is a peculiar supernova, but that may be due to its being observed close to the axis of its GRB emission. It is not out of the question that a good fraction —perhaps *all*— of the core-collapse SNe be associated with GRBs. To make the total cosmic rate of GRBs and SN compatible, this nearly one-to-one GRB/SN association would require beaming into a solid angle that is a fraction  $f \sim 2 \times 10^{-6}$  of  $4\pi$  [12]. The CB model, for the emission from CBs moving with  $\gamma \sim 10^3$ , implies precisely that beaming factor (the numerical details are reproduced in Section 9).

*The GRB engine.* We assume a core-collapse SN event not to result only in the formation of a central compact object and the expulsion of a supernova shell (SNS). A fraction of the parent star’s material, external to the newly-born compact object, should fall back in a time very roughly of the order of one day [12] and, given the considerable specific angular momentum of stars, it should settle into an accretion disk and/or torus around the compact object<sup>1</sup>. The subsequent sudden episodes of accretion —occurring with a time sequence that we cannot predict— result in the emission of CBs. These emissions last till the reservoir of accreting matter is exhausted. The emitted CBs initially expand in the SN rest-system at a speed  $\beta c/\gamma$ , with  $\beta c$  presumably of the same order or smaller than the speed of sound in a relativistic plasma ( $\beta = 1/\sqrt{3}$ ). The solid angle a CB subtends is so small that presumably successive CBs do not hit the same point of the outgoing SNS, as they catch up with it. These considerations are illustrated in Fig.(1).

*The GRB.* From this point onwards, the CB model is not based on analogies or assumptions, but on processes whose outcome can be approximately worked out in an explicit manner. The violent collision of the CB with the SNS heats the CB (which is not transparent at this point to  $\gamma$ ’s from  $\pi^0$  decays) to a temperature that, by the time the CB reaches the transparent outskirts of the SNS, is  $\sim 150$  eV, further decreasing as the CB travels [22]. The resulting CB surface radiation, Doppler-shifted in energy and forward-collimated by the CB’s fast motion, gives rise to an individual pulse in a GRB, as illustrated in Fig.(1). The GRB light curve is an ensemble of such pulses, often overlapping one another. The energies of the individual GRB  $\gamma$ -rays, as well as their typical total fluences, indicate CB Lorentz factors of  $\mathcal{O}(10^3)$ , as the SN/GRB association does [22]. The GRB properties most relevant to the current investigation are reviewed in Section 5.

---

<sup>1</sup>We choose to base our conjectures on analogies with known processes, as opposed to computer simulations. The latter do not yet realistically include rotation, magnetic fields, the transport of angular momentum... Most noticeably, they do not produce SN explosions.

*The GRB's afterglow.* The CBs, after they exit the SNS, cool down by bremsstrahlung and radiate by this process, by inverse Compton scattering, and by synchrotron radiation of their electrons on their enclosed magnetic field, much as the plasmoids emitted by quasars and microquasars do [12]. The CB model provides an excellent detailed description of optical afterglows [13]. The early afterglow spectrum and light curve are complicated by the fact that, about a day after the GRB emission, CBs cool down to a temperature at which e-p recombination into H takes place. This gives rise to Ly- $\alpha$  lines that the CB's motion Doppler-shifts to (cosmologically redshifted) energies of order a few keV, an energy domain that, interestingly, coincides with that of the Fe lines that an object at rest would emit. Recombination also gives rise to a multiband-flare in the afterglow. These CB-model's expectations are in good agreement with incipient data on X-ray lines and flares [23].

In all of the above considerations we have exploited the GRB/SN association to conclude that GRBs, at least the long duration ones, are associated with core-collapse SNe. This allows us to be very specific in our predictions [12, 22, 23] concerning the collision of the CBs with the SNS, and the consequent properties of the GRB pulses (the density profile of SNSs is known from observations; the typical energy of CBs we can infer from the assumption that the large peculiar velocities of neutron stars are due to an imbalance between the momenta of the jets of CBs they emit as they are born [11]). But the sites of GRB emission may not be only SNe. Any process of violent accretion, such as a merger between neutron stars or other compact objects, may result in the emission of CBs. If the latter encounter matter on their way, such as circumstellar gas or a molecular cloud, the processes leading to  $\gamma$ -ray emission would be similar to the ones pertaining to a SN engine.

In this paper we address two other concrete predictions of the Cannonball Model: the emission of neutrinos and of energetic  $\gamma$ -rays (EGRs). Once again, to be specific, we exploit our explicit model of GRBs emitted in core-collapse SN events. The neutrinos are made by the chain decays of charged pions, produced in the collisions of the CBs' baryons with those of the SNS, as in Fig.(1). The  $\nu$  beam carries almost all of the emitted energy, but is much narrower than the GRB beam and should only be detected in coincidence with the small fraction of GRBs whose CBs are moving extremely close to the line of sight. The EGRs are made by the decay of neutral pions, but only from  $\pi^0$  production close enough to the outskirts of the SNS for the  $\gamma$ -rays not to be subsequently absorbed, see Fig.(1). The EGR beam, whose fluence is comparable to that of the GRB, is as wide as the GRB beam and should be observable, in coincidence with GRBs, with existing or planned detectors. The EGR beam peaks at energies of tens of GeVs, while the  $\nu$  beam is about one order of magnitude more energetic.

## 2 Times and energies

Let  $\gamma = 1/\sqrt{1 - \beta^2} = E_{\text{CB}}/(M_{\text{CB}}c^2)$  be the Lorentz factor of a CB, which diminishes with time as the CB hits the SNS and as it subsequently plows through the interstellar medium. Four clocks ticking at different paces are relevant to a CB's history. Let  $t_{\text{SN}}$  be the local time in the SN rest system,  $t_{\text{CB}}$  the time in the CB's rest system,  $t_{\text{Ob}}$  the time measured by a nearby observer viewing the CB at an angle  $\theta$  away from its direction of motion, and  $t$  the time measured by an earthly observer viewing the CB at the same angle, but from a “cosmological” distance (redshift  $z \neq 0$ ). Let  $x$  be the distance traveled by the CB in the SN rest system. The relations between the above quantities are:

$$\begin{aligned} dt_{\text{SN}} &= \gamma dt_{\text{CB}} = \frac{dx}{\beta c}; \\ dt_{\text{CB}} &\equiv \delta dt_{\text{Ob}}; \\ dt &= (1 + z) dt_{\text{Ob}} = \frac{1 + z}{\gamma \delta} dt_{\text{SN}}, \end{aligned} \quad (1)$$

where the Doppler factor  $\delta$  is:

$$\delta \equiv \frac{1}{\gamma(1 - \beta \cos \theta)} \simeq \frac{2\gamma}{(1 + \theta^2\gamma^2)}, \quad (2)$$

and its approximate expression is valid for  $\theta \ll 1$  and  $\gamma \gg 1$ , the domain of interest here. Notice that for large  $\gamma$  and not large  $\theta\gamma$ , there is an enormous “relativistic aberration”:  $dt \sim dt_{\text{SN}}/\gamma^2$ , and the observer sees a long CB story as a film in extremely fast motion.

The energy of the photons radiated by a CB in its rest system,  $E_{\text{CB}}^\gamma$ , their energy in the direction  $\theta$  in the local SN system,  $E_{\text{SN}}^\gamma$ , and the photon energy  $E$  measured by a cosmologically distant observer, are related by:

$$E_{\text{CB}}^\gamma = \frac{E_{\text{SN}}^\gamma}{\delta}; \quad E_{\text{SN}}^\gamma = (1 + z) E, \quad (3)$$

with  $\delta$  as in Eq.(2).

## 3 Reference values of various parameters

To be explicit we must scale our results to given values of the parameters of the CB model. In this section we introduce the reference values that we adopt, which serve as benchmarks but imply no strong commitment to their particular choices. These values are listed in Table I, for quick reference.

Parameter	Symbol	Value
SN-shell’s mass	$M_S$	$10 M_\odot$
SN-shell’s radius	$R_S$	$2.6 \times 10^{14}$ cm
Outgoing Lorentz factor	$\gamma_{\text{out}}$	$10^3$
CB’s energy	$E_{\text{CB}}$	$10^{52}$ erg
Initial $v_T/c$ of expansion	$\beta_{\text{in}}$	$1/(3\sqrt{3})$
Final $v_T/c$ of expansion	$\beta_{\text{out}}$	$1/\sqrt{3}$
Redshift	$z$	1
CB’s viewing angle	$\theta$	$10^{-3}$

Table 1: List of the “reference” values of various parameters. In the text a barred parameter means its actual value divided by its reference value, so that, for instance,  $\bar{M}_S = 1/2$  means that the actual mass of the SN shell is taken to be  $5 M_\odot$ . Two parameters are not specific to our model ( $z$  and  $\theta$ ).

Let “jet” stand for the ensemble of CBs emitted in one direction in a SN event. If a momentum imbalance between the opposite-direction jets is responsible for the large peculiar velocities of neutron stars,  $v_{\text{NS}} \approx 450 \pm 90$  km s<sup>-1</sup> [29], the jet kinetic energy  $E_{\text{jet}}$  must be, as we shall assume for our GRB engine, larger than  $M_{\text{NS}} v_{\text{NS}} c \sim 10^{52}$  erg, for  $M_{\text{NS}} = 1.4 M_\odot$  [11]. We adopt a value of  $10^{53}$  ergs as the reference jet energy<sup>2</sup>. On average, GRBs have some five to ten significant pulses, so that the energy in a single CB may be 1/5 or 1/10 of  $E_{\text{jet}}$ . We adopt  $E_{\text{CB}} = 10^{52}$  erg as our reference value. We denote with a bar the actual value of a parameter in the units of its reference value so that  $\bar{E}_{\text{CB}}$ , for instance, means a given cannonball energy divided by  $10^{52}$  erg.

Let  $\gamma_{\text{in}}$  be the Lorentz factor of a cannonball as it is fired. We shall find  $\gamma_{\text{in}} = \mathcal{O}(3 \times 10^3)$  to be a “typical” value ( $\gamma_{\text{in}}$  is not an “input” parameter). For this value and the reference CB energy, the CB’s mass is very small by stellar standards, and comparable to an Earth mass:

$$M_{\text{CB}} \sim 0.6 M_\oplus \frac{3 \times 10^3}{\gamma_{\text{in}}}. \quad (4)$$

The baryonic number of the CB is:

$$N_b \simeq \frac{E_{\text{CB}}}{m_p c^2 \gamma_{\text{in}}} \simeq 2.2 \times 10^{51} \bar{E}_{\text{CB}} \left[ \frac{3 \times 10^3}{\gamma_{\text{in}}} \right]. \quad (5)$$

The collision of a CB with a SNS is so violent —at  $\sim 1$  TeV per nucleon— that

---

<sup>2</sup>The jet-emitting process may be “up-down” symmetric to a good approximation, implying even bigger jet energies. In the accretion of matter by black holes in quasars [30, 31] and micro-quasars [24] the efficiency for the conversion of gravitational binding energy into jet energy appears to be surprisingly large. If in the production of CBs the central compact object ingurgitates several solar masses,  $E_{\text{jet}}$  could be as large as  $\sim M_\odot c^2 \simeq 1.8 \times 10^{54}$  erg.

there is no doubt that, as it exits the shell, the CBs' baryonic number resides in individual protons and neutrons.

We have assumed that, in a SN explosion, some of the material outside the collapsing core is not expelled as a SNS, but falls back onto the compact object. For vanishing angular momentum, the free-fall time of a test-particle from a distance  $R$  onto an object of mass  $M$  is  $t_{\text{fall}} = \pi [R^3/(8GM)]^{1/2}$ . For material falling from a typical star radius ( $R_{\star} \sim 10^{12}$  cm) on an object of mass  $M = 1.4 M_{\odot}$ ,  $t_{\text{fall}} \simeq 1$  day. The fall-time is longer (except for material falling from the polar directions) if the specific angular momentum is considerably large, as it is in most stars. The fall-time is shorter for material not falling from as far as the star's radius. The estimate  $t_{\text{fall}} \simeq 1$  day is therefore a very rough one. One day after core-collapse, the expelled SNS, traveling at a velocity  $v_S \sim c/10$  [32], has moved to a distance:

$$R_S = 2.6 \times 10^{14} \text{ cm} \left( \frac{t_{\text{fall}}}{1 \text{ d}} \right) \left( \frac{10 v_S}{c} \right). \quad (6)$$

We adopt  $R_S = 2.6 \times 10^{14}$  cm as our reference value.

For the Lorentz factor of the CBs as they exit the SNS, we adopt the value  $\gamma_{\text{out}} = 10^3$ , for the reasons discussed in the Introduction. Let  $\beta_{\text{in}} c$  be the expansion velocity of a CB, in its rest system, as it travels from the point of emission to the point at which it reaches the SNS, and let  $\beta_{\text{out}} c$  be the corresponding value after the CB exits the SNS, reheated by the collision. We expect these velocities to be comparable to the speed of sound in a relativistic plasma,  $c/\sqrt{3}$ , as observed in the initial expansion of the CBs emitted by GRS 1915+105 [24]. As reference values, we adopt those of Table I.

## 4 The collision of a CB with the SNS

### 4.1 The shell's profile and transparency

The density profile of the transparent outer layers of a SNS as a function of the distance  $x$  to the SN centre can be inferred from the photometry, spectroscopy and evolution of the SN emissions [32]. The observations can be fit by a power law,  $x^{-n}$ , with  $n \sim 4$  to 8. Our results for neutrino fluxes are not sensitive to this density profile and our results for GRB  $\gamma$ -rays [22] and for EGRs are only sensitive to the outer region where the SN shell becomes transparent. This implies that, for simplicity, we can adopt at all  $x > R_S$  the density profile observed in the shell's outer layers:

$$\rho(x) = \rho(R_S) \Theta(x - R_S) \left[ \frac{R_S}{x} \right]^n. \quad (7)$$

The SNS grammage still in front of a CB located at  $x$  is:

$$X_S(x) = \int_x^\infty \rho(y) dy = X_{\text{SNS}} \left[ \frac{R_S}{x} \right]^{n-1}$$

$$X_{\text{SNS}} \equiv \frac{M_S}{4\pi R_S^2} \simeq (2.35 \times 10^4) \frac{\bar{M}_S}{\bar{R}_S^2} \text{ g cm}^{-2}. \quad (8)$$

For GRB photons in the MeV domain the attenuation length is similar, within a factor 2, in all elements from H to Fe, and it is close to the attenuation length in a hydrogenic plasma. In the CB model, at a fixed time, the energy spectrum in a GRB pulse is roughly thermal [22]. The radiation length in the obscuring shell, averaged over a black body spectrum of peak energy 1 MeV, is approximately:

$$X_{\text{GRB}} \simeq \frac{m_p}{\sigma_{\text{KN}}(1 \text{ MeV})} \simeq 10 \text{ g cm}^{-2}, \quad (9)$$

where  $\sigma_{\text{KN}}$  is the Klein-Nishina cross section. For EGRs the attenuation length in hydrogen in the 100 MeV to 100 GeV range, dominated by  $e^+e^-$  pair production, is [33]:

$$X_{\text{EGR}} \simeq 70 \text{ gr cm}^{-2}. \quad (10)$$

The attenuation lengths of Eqs.(9) and (10) are all much smaller than the typical shell grammage of Eq.(8).

Equating  $X_S(x)$  and  $X_{\text{GRB}}$  and solving for  $x$ , one obtains the radial distance  $x_{\text{GRB}}^{\text{tp}}$  at which the SNS becomes (one radiation length) transparent to GRB photons. For our reference parameters, some representative results are:

$$x_{\text{GRB}}^{\text{tp}}/R_S \simeq (3.7, 6.2, 21) \quad \text{for } n = (8, 6, 4). \quad (11)$$

The corresponding values for  $x_{\text{EGR}}^{\text{tp}}$ , at a given  $n$ , are shorter:

$$x_{\text{EGR}}^{\text{tp}}/R_S \simeq (2.3, 3.2, 6.9) \quad \text{for } n = (8, 6, 4). \quad (12)$$

The GRB and EGR signals are emitted as the CB reaches the transparent outskirts of the SNS. The neutrino signal is emitted as soon as the CB starts colliding with the shell. We discuss in detail in Section 10 the time profiles and relative timing of these signals.

## 4.2 Kinematics of a CB's collision with a SN shell

The radius of the expanding CBs, as they reach the SNS, is:

$$R_{\text{CB}} \sim R_S \frac{\beta_{\text{in}}}{\gamma_{\text{in}}} \simeq 1.7 \times 10^{10} \text{ cm } \bar{\beta}_{\text{in}} \left[ \frac{3 \times 10^3}{\gamma_{\text{in}}} \right] \bar{R}_S, \quad (13)$$



In its collision with the shell, a CB sweeps up a “target” mass

$$M_T \sim \pi R_{\text{CB}}^2 X_{\text{SNS}} = M_S \frac{\beta_{\text{in}}^2}{4 \gamma_{\text{in}}^2} \simeq 3.5 \times 10^{-3} M_{\otimes} \bar{\beta}_{\text{in}} \left[ \frac{3 \times 10^3}{\gamma_{\text{in}}} \right]^2 \bar{M}_S, \quad (14)$$

where  $X_{\text{SNS}}$  is the full column density of the shell, as in Eq.(8).

Seen from the reference system in which the CB is at rest (and its shape, because of expansion, is roughly spherical) the constituents of the SNS impinge onto the CB with a Lorentz factor  $\gamma_{\text{in}}$ . The average density of a CB with the reference radius of Eq.(13) and the reference mass of Eq.(4) is  $\rho \sim 1.8 \times 10^{-4} \text{ gr cm}^{-3}$ . The nucleon–nucleon interaction length at that density is  $\lambda_{\text{CB}} = (N_A \sigma_{\text{pp}}^{\text{TOT}} \rho)^{-1} \sim 2.2 \times 10^5 \text{ cm}$ , with  $N_A$  Avogadro’s number and  $\sigma_{\text{pp}}^{\text{TOT}} \simeq 40 \text{ mb}$  the proton–proton (or nucleon–nucleon) cross section at TeV beam energies. The CB’s radius of Eq.(13) is much bigger than  $\lambda_{\text{CB}}$ , implying that all nuclei in the region of the shell swept up by the CB interact. Approximately 1/3 of the energy in these collisions results in photons from  $\pi^0$  decay, which heat the CB to a temperature in the keV domain [12, 22].

Seen from the reference system in which the SNS is at rest (or moving with a modestly relativistic velocity  $\sim c/10$ ) a high-energy nucleon in the CB —suffering successive interactions in the dilute gas or plasma constituting the SNS— loses roughly 2/3 of its energy to  $\pi^\pm$  production. The density of the shell is of order  $\rho_S = M_S/(4 \pi R_S^3) \sim 10^{-10} \text{ gr/cm}^3$ , for our typical parameters. At that density, the nucleon-nucleon interaction length is  $\lambda_S \sim 5 \times 10^{11} \text{ cm}$ , much less than the  $\mathcal{O}(R_S)$  shell’s depth, so that the shell’s material is, in this sense, “thick”: it acts as a beam dump. The decay length of a charged pion of energy  $E_\pi$  is  $5.6 \times 10^5 E_\pi/(100 \text{ GeV}) \text{ cm}$ , much less than its interaction length, which is comparable to that of nucleons. Consequently, the beam dump is “thin” to  $\pi$  decay and roughly 2/3 of a CB’s nucleon energy is carried away by the neutrinos in  $\pi \rightarrow \mu \nu$  decays and in the subsequent  $\mu$  decays.

The Lorentz factor of the CB after it has swept the SNS is simply the ratio of the total energy to the invariant mass of the outgoing object:

$$\gamma_{\text{out}} \simeq \frac{E_{\text{CB}}/3}{\sqrt{2 M_T c^2 E_{\text{CB}}/3 + M_{\text{CB}}^2 c^4}}, \quad (15)$$

where we have used  $E_{\text{CB}} \gg M_T c^2$ , with  $M_T$  the target mass of Eq.(14). Substituting for  $M_T$  and  $M_{\text{CB}}$  as functions of  $\gamma_{\text{in}}$  and  $\beta_{\text{in}}$ , one obtains:

$$\gamma_{\text{out}} \simeq \gamma_{\text{in}} \sqrt{\frac{2 E_{\text{CB}}}{3 \beta_{\text{in}}^2 M_S c^2 + 18 E_{\text{CB}}}} \quad (16)$$

whose limiting values are:

$$\begin{aligned} \gamma_{\text{out}} &\sim \frac{\gamma_{\text{in}}}{3} \quad (\text{for } 6 E_{\text{CB}} \gg \beta_{\text{in}}^2 M_S c^2) \\ \gamma_{\text{out}} &\sim \frac{\gamma_{\text{in}}}{10 \bar{\beta}_{\text{in}}} \left[ \frac{\bar{E}_{\text{CB}}}{\bar{M}_S} \right]^{\frac{1}{2}} \quad (\text{for } 6 E_{\text{CB}} \ll \beta_{\text{in}}^2 M_S c^2). \end{aligned} \quad (17)$$

For our reference parameters, Eq.(16) implies that  $\gamma_{\text{in}} \sim 10 \gamma_{\text{out}}$ . The very large “typical” values of  $\gamma_{\text{in}}$ ,  $\sim 3 \times 10^3$  or larger, as in Eqs.(17), imply that the fractional solid angle covered by a CB as it hits the SNS is tiny:  $\beta_{\text{in}}^2/(4 \gamma_{\text{in}}^2) \sim 10^{-9}$  or smaller, for our reference  $\beta_{\text{in}}$ . This presumably makes it unlikely for consecutive CBs to hit precisely the same spot in the SNS: CB–CB collisions and mergers may be the exception, rather than the rule, and the collisional “histories” of successive CBs should be similar.

Let  $\sigma_{\text{T}} \simeq 6.5 \times 10^{-25} \text{ cm}^2$  be the Thomson cross section, describing  $\gamma$ -e collisions at invariant masses comparable or smaller than the electron mass. The CB itself becomes transparent to the radiation it encloses when it reaches a radius  $R_{\text{CB}}^{\text{tp}} \simeq [3 M_{\text{CB}} \sigma_{\text{T}} / (4 \pi m_{\text{p}})]^{\frac{1}{2}} \sim 1.9 \times 10^{13} \text{ cm}$ , for  $M_{\text{CB}} = 0.6 M_{\odot}$ . If the CB in its rest system, after the collision with the SNS, is expanding at a transverse velocity  $\beta_{\text{out}} c$ , the distance away from the SN at which it becomes transparent is  $\gamma_{\text{out}} R_{\text{CB}}^{\text{tp}} / \beta_{\text{out}}$ , or  $\sim 3.3 \times 10^{16} \text{ cm}$  for our reference parameters. By then, the CB is well out of the SNS and it has emitted from its expanding surface the radiation that constitutes the GRB signal [22].

### 4.3 Microscopic description of the collision

The main point in outlining a microscopic picture of the collision of a CB and a SNS, as we shall see, is to conclude that the details of such a picture are immaterial to the estimate of the properties of GRBs and of their associated EGR- and high-energy  $\nu$  fluxes. But the discussion is important in that it sets the basis for *how* to make these estimates.

Both the SNS and the CB are many pp interaction lengths long. The number of such lengths in the SNS is:

$$N_{\text{SNS}}^{\text{int}} = \frac{M_{\text{S}} N_{\text{A}}}{\pi R_{\text{S}}^2} \sigma_{\text{pp}}^{\text{TOT}} \simeq (5.6 \times 10^2) \bar{M}_{\text{S}} [\bar{R}_{\text{S}}]^{-2}, \quad (18)$$

As it enters the shell at a distance  $x = R_{\text{S}}$  from the SN centre, the number of pp interaction lengths in the CB is:

$$N_{\text{CB}}^{\text{int}} \sim \frac{M_{\text{CB}} N_{\text{A}}}{\pi R_{\text{CB}}^2} \sigma_{\text{pp}}^{\text{TOT}} \simeq (1.6 \times 10^5) \bar{E}_{\text{CB}} \left[ \frac{\gamma_{\text{in}}}{3 \times 10^3} \right]^2 [\bar{\beta}_{\text{in}} \bar{R}_{\text{S}}]^{-2}. \quad (19)$$

At a later point in the crossing of the SNS, e.g. at  $x = 2 R_{\text{S}}$ , when the CB is moving at  $\gamma \sim \gamma_{\text{out}}$  and expanding at a speed  $\beta_{\text{out}}$ , its number of interaction lengths is:

$$\tilde{N}_{\text{CB}}^{\text{int}} \sim (5.1 \times 10^2) \bar{E}_{\text{CB}} [\bar{\gamma}_{\text{in}}]^{-1} [\bar{\gamma}_{\text{out}}]^2 [\bar{\beta}_{\text{out}} \bar{R}_{\text{S}}]^{-2}. \quad (20)$$

Thus, the number of pp interaction lengths in the CB is typically comparable to or bigger than the corresponding number in the SNS.

The simplest reference system in which to visualize the collision is the centre-of-mass system (c.m.s.) of two slabs of nuclei, one belonging to the CB, the other to the SNS, both one interaction length long. Consider first the case in which the CB and the SNS are an equal number of nucleon–nucleon interaction lengths long. In the approximation of constant densities, the slab–slab c.m.s. coincides in this case with the overall c.m.s. of the CB and the material that it hits in the SNS<sup>3</sup>. In this system both the CB and the shell are spatially contracted (relative to their respective rest systems) by the Lorentz factor  $\sqrt{\gamma_{\text{in}}}/2$  at which their constituents are moving towards each other. After the nucleons have interacted once, their energy is degraded by an average factor  $f \sim 0.7$ , (the “leading particle” average-energy fraction observed in high-energy nuclear collisions). The nucleons of the leading slab, after the time required to interact a few times with a few “opposing” slabs, come to rest and are eventually turned back. Meanwhile fresh slabs are coming in and suffering the same fate as the first. An increasingly hot and dense pancake-shaped region is formed, containing the nucleons that have collided and the radiation initiated by  $\gamma$ ’s from  $\pi^0$  decay. Because of its enclosed radiation pressure, this “pancake” eventually expands in its rest system at a speed of  $\mathcal{O}(c/\sqrt{3})$ . When all the slabs of the CB and of the SNS are consumed, the resulting object is the outgoing CB, at rest in this system.

In the case where the number of interaction lengths in the CB and the SNS are different, a similar description applies in the system of reference in which the CB and shell densities are the same, up to the moment in which the object with the smaller number of interaction lengths is consumed. This object is typically the SNS, as Eqs.(18) to (20) indicate. At that point, we have a hot and dense pancake-shaped object at rest, plus the fresh slabs from the CB’s side of the collision that are impinging on the disk without having interacted yet. As these fresh slabs hit, they set the disk in motion. The final outgoing CB, now viewed from the local rest system of the parent SN, is moving with the Lorentz factor  $\gamma_{\text{out}}$  of Eq.(16).

No doubt the previous description is oversimplified, for the violence of the collision of the CB and the SNS presumably results in shocked and turbulent motions. Moreover, the freshly expelled SNS is probably not smooth, but also turbulent and inhomogeneous on small scales. Fortunately, a detailed description is not required for an estimate of the fluxes of  $\nu$ ’s and EGRs.

---

<sup>3</sup>It is easy to generalize the argument that follows to non-constant densities, by using a variable reference system in which the densities are instantaneously the same, but that requires an unjustified amount of effort, the final results on the observable  $\nu$  fluxes being the same. The generalization to unequal numbers of interaction lengths, we shall deal with explicitly.

## 5 The GRB

In this section we briefly review the properties<sup>4</sup> of GRBs, in the CB model [22], that we need to establish comparisons between the GRB itself, and its accompanying EGR and  $\nu$  fluxes.

In its rest frame, the front surface of a CB is bombarded by the nuclei of the SNS, which have an energy  $m_p c^2 \gamma \sim 1$  TeV per nucleon, roughly 1/3 of which is converted into  $\gamma$ -rays (from  $\pi^0 \rightarrow \gamma\gamma$  decays) within a nucleon attenuation length:

$$X_p = \frac{m_p}{\sigma_{pp}^{\text{TOT}}} \simeq 42 \text{ g cm}^{-2}. \quad (21)$$

These high energy photons initiate electromagnetic cascades that, in turn, convert their energy to thermal energy within the CB. The radiation length of high energy  $\gamma$ 's in hydrogenic plasma is  $X_{\text{EGR}}$ , given by Eq.(10). The energy of the electromagnetic cascade ends up as heat. The thermal photons, of energy  $E_\gamma \ll m_e c^2$ , have a radiation length:

$$X_T \simeq \frac{m_p}{\sigma_T} \simeq 2.6 \text{ g cm}^{-2}. \quad (22)$$

The thermal energy contained in a CB's front-surface layer of "depth"  $X_T$ , continually supplied by the SNS incident nucleons, will be radiated away. It is reasonable to expect that an equilibrium is established whereby, to a fair approximation, the quasi-thermal emission rate from the CB is in equilibrium with the fraction of energy deposited by the CB's collision with the SN shell within this one-radiation deep layer. A fraction  $X_T/X_p$  of the incoming protons interact in the radiating layer, and a fraction  $X_T/X_{\text{EGR}}$  of the energy of the  $\gamma$ s from  $\pi^0$  production and decay is deposited in it. The total energy deposited by a single SNS shell nucleon is  $\sim m_p c^2 \gamma/3$ . Equating the energy deposition per unit time to that re-emitted from the CB's surface as quasi-thermal radiation, we obtain an instantaneous temperature:

$$T(x) \simeq \left[ \frac{X_T^3}{X_p X_{\text{EGR}}} \frac{(n-1) c^3 [\gamma(x)]^2}{6 \sigma x_{\text{GRB}}^{\text{tp}}} \right]^{1/4} \left[ \frac{x}{x_{\text{GRB}}^{\text{tp}}} \right]^{-n/4}, \quad (23)$$

where  $\sigma$  is the Stefan–Boltzmann constant,  $\gamma(x)$  is a function evolving from  $\gamma_{\text{in}}$  to  $\gamma_{\text{out}}$ ,  $x_{\text{GRB}}^{\text{tp}}$  is as in Eqs.(11), and  $n$  is the SNS density index of Eq.(7). The temperature as the CB reaches the transparent region of the SNS,  $T_{\text{tp}} \equiv T(x_{\text{GRB}}^{\text{tp}})$ , is of order 0.15 keV, and is not very sensitive to the parameters of the model [22], scaling roughly as:

$$T_{\text{tp}} \propto \left[ \frac{n-1}{R_S} \right]^{1/4} [\gamma_{\text{out}}]^{1/2}, \quad (24)$$

since  $x_{\text{tp}} \propto R_S$  and, in the outer regions of the SNS,  $\gamma(x) \sim \gamma_{\text{out}}$ .

---

<sup>4</sup>We use the "surface model" of [22].

The time-width of a single-CB GRB pulse is roughly characterized by a “transparency time”  $t_{\text{GRB}}$ : the time elapsed between the moment the CB enters the SNS and the time it reaches its (one radiation length) transparent outer layer. In the observer’s frame, this time is:

$$t_{\text{GRB}} \simeq \frac{1+z}{\gamma_{\text{out}} \delta} \frac{x_{\text{GRB}}^{\text{tp}} - R_{\text{S}}}{c}, \quad (25)$$

with  $x_{\text{GRB}}^{\text{tp}}$  as in Eq.(11). For our standard parameters and a typical  $\theta \sim 3/\gamma_{\text{out}}$ ,  $t_{\text{GRB}}$  is  $\sim 0.23, 0.45, 1.7$  s, for SNS indices  $n = 8, 6, 4$ , respectively.

The radius of the CB at the time  $t = t_{\text{GRB}}$  is:

$$R_{\text{CB}}^{\text{tp}} \sim R_{\text{CB}} + (x_{\text{GRB}}^{\text{tp}} - R_{\text{S}}) \frac{\beta_{\text{out}}}{\gamma_{\text{out}}} \quad (26)$$

with  $R_{\text{CB}}$  as in Eq.(13). For times of  $\mathcal{O}(t_{\text{GRB}})$ , the radius of the CB increases approximately linearly with time. In the CB’s rest system, and at a fixed time, the energy spectrum of the radiation emitted by the CB is an approximate black-body spectrum, corrected for absorption in the SNS, and emitted by a sphere whose surface grows as  $t^2$  and whose surface temperature decreases as  $[t_{\text{GRB}}/t]^{(n/2)}$ , as in Eq.(23). We have shown in [22] that this simple picture describes well the light curves and energy spectra of GRB pulses. The predicted GRB energy spectrum is the sum of thermal spectra with decreasing temperatures. Its high energy tail is exponential, with a characteristic temperature  $\sim T_{\text{tp}}$ . At high energies, this is an underestimate with respect to the observed GRB spectra, which decrease approximately as  $E^{-2}$ . We attribute this discrepancy to the naiveté of our thermal input spectrum: observations demonstrate that astrophysical plasmas subject to a flux of high energy particles —such as the CB in its rest system— radiate a “quasi-thermal” spectrum, corrected at high energies for such a power-law tail (clusters of galaxies are discussed in [34], galaxy groups in [35] and SN remnants in [36]).

To estimate the total energy radiated by a CB’s heated surface we must first compute the number  $N_{\text{p}}^{\text{GRB}}$  of SNS nucleons that provide this energy, with the constraint that the radiation they eventually produce be able to escape from the SNS. The naive estimate  $N_{\text{p}}^{\text{GRB}} \simeq \pi [R_{\text{CB}}^{\text{tp}}]^2 X_{\text{GRB}}/m_{\text{p}}$  turns out to be a very good approximation. Indeed, in terms of  $n_{\text{p}}(x)$ , the nucleon number density in the shell, and  $X_{\text{SNS}} = X_{\text{S}}(R_{\text{S}})$ , the shell’s total grammage of Eq.(8),  $N_{\text{p}}^{\text{GRB}}$  is:

$$\begin{aligned} N_{\text{p}}^{\text{GRB}} &= \int_{R_{\text{S}}}^{\infty} dx \pi [R_{\text{CB}}(x)]^2 n_{\text{p}}(x) \text{Exp} \left[ -\frac{m_{\text{p}}}{X_{\text{GRB}}} \int_x^{\infty} n_{\text{p}}(x') dx' \right] \\ &= \pi \frac{X_{\text{GRB}}}{m_{\text{p}}} \int_{R_{\text{S}}}^{\infty} dx [R_{\text{CB}}(x)]^2 \frac{d}{dx} \text{Exp} \left[ -\frac{m_{\text{p}}}{X_{\text{GRB}}} \int_x^{\infty} n_{\text{p}}(x') dx' \right] \\ &\approx \pi [R_{\text{CB}}^{\text{tp}}]^2 \frac{X_{\text{GRB}}}{m_{\text{p}}} (1 - \text{Exp}[-X_{\text{S}}/X_{\text{GRB}}]) \approx \pi [R_{\text{CB}}^{\text{tp}}]^2 \frac{X_{\text{GRB}}}{m_{\text{p}}}, \quad (27) \end{aligned}$$

where we have approximated by a constant the radius of the CB as it travels through the outer few GRB absorption lengths. In the CB's rest frame, the total radiated energy is:

$$E_{\text{pulse}}^{\text{rest}} \approx \frac{X_{\text{GRB}} X_{\text{T}}^2}{X_{\text{EGR}} X_{\text{p}}} \frac{\pi [R_{\text{CB}}^{\text{tp}}]^2 c^2 \gamma_{\text{out}}}{3}. \quad (28)$$

As an example, for our standard parameters and  $n = 8$ ,  $R_{\text{CB}}^{\text{tp}} \sim 4 \times 10^{11}$  cm and  $E_{\text{pulse}}^{\text{rest}} \sim 3 \times 10^{45}$  erg. The result scales roughly as  $R_{\text{S}}^2 \beta_{\text{out}}^2 / \gamma_{\text{out}}$  and could be one or two orders of magnitude smaller for  $R_{\text{S}}$  and  $\beta_{\text{out}}$  somewhat below our reference values.

An observer at rest, located at a known luminosity distance  $D_{\text{L}}(z)$  from the CB and viewing it at an angle  $\theta$  from its direction of motion, would measure a “total” (time- and energy-integrated) fluence per unit area:

$$\frac{df}{d\Omega} \simeq \frac{1+z}{4\pi D_{\text{L}}^2} E_{\text{pulse}}^{\text{rest}} \left[ \frac{2\gamma_{\text{out}}}{1+\theta^2\gamma_{\text{out}}^2} \right]^3. \quad (29)$$

In a critical ( $\Omega = 1$ ) Friedman universe the luminosity distance is given by:

$$D_{\text{L}}(z) = \frac{(1+z)c}{H_0} \int_{\frac{1}{1+z}}^1 \frac{dx}{\sqrt{\Omega_{\Lambda} x^4 + \Omega_{\text{M}} x}}, \quad (30)$$

where  $H_0$  is Hubble's parameter,  $\Omega_{\text{M}}$  and  $\Omega_{\Lambda} = \Omega - \Omega_{\text{M}}$ , respectively, are the matter and vacuum energy densities divided by the critical density ( $\rho_{\text{c}} = 3H_0^2/8\pi G$ ) and the radiation energy density has been neglected. In our explicit calculations we use  $H_0 = 65$  km/(s Mpc),  $\Omega_{\text{M}} = 0.3$  and  $\Omega_{\Lambda} = 0.7$ , so that, for example,  $D_{\text{L}}(1) \simeq 7.12$  Gpc  $\simeq 2.20 \times 10^{28}$  cm. In Fig.(2) we show  $D_{\text{L}}(z)$  and  $[D_{\text{L}}(1)/D_{\text{L}}(z)]^2$  (the quantity to which we shall scale our results) for the quoted cosmology and, for comparison, for the case  $\Omega_{\text{M}} = 1$ ,  $\Omega_{\Lambda} = 0$ , for which  $D_{\text{L}}(1) \simeq 5.41$  Gpc  $\simeq 1.67 \times 10^{28}$  cm.

## 6 The sources of high energy particles

### 6.1 The origin of high energy $\nu$ 's

The nuclei or nucleons in the incoming CB are comoving with it with a Lorentz factor  $\gamma_{\text{in}}$ . Nuclei in the outgoing CB have certainly been shattered into their constituent nucleons by the violence of the collision between the CB and the shell. They are comoving with the bulk Lorentz factor  $\gamma_{\text{out}}$ . On average, a high energy nucleon colliding at a large centre-of-mass energy with a nucleon at rest—or moving along the same direction—exits the collision with a small transverse momentum and a fraction  $f \sim 0.7$  of its original energy (for ultrarelativistic particles this statement is independent of longitudinal Lorentz boosts). The nucleons of the incoming CB must

have their Lorentz factor degraded from  $\gamma_{\text{in}}$  to  $\gamma_{\text{out}}$ . On average, this takes a number  $i$  of high-energy collisions satisfying  $f^i = \gamma_{\text{out}}/\gamma_{\text{in}}$ , that is  $i \sim 3$ , for  $\gamma_{\text{in}} \sim 3 \gamma_{\text{out}}$ , or  $i \sim 6$ , for  $\gamma_{\text{in}} \sim 10 \gamma_{\text{out}}$ .

Another way to reach a conclusion similar to the above is to view the interactions in the reference system introduced in Section 4.3. There we saw that the bulk of the CB's nucleons impinge, with a Lorentz factor  $\sqrt{\gamma_{\text{in}}}/2$ , on a “pancake”, which is at rest, or moving towards them at a mildly relativistic velocity  $\sim c/\sqrt{3}$ . For  $\gamma_{\text{in}} = 3 \times 10^3$  ( $10^4$ ) the incoming energy of the CB's nucleons is  $E \sim 26$  GeV ( $\sim 47$  GeV). Consider the number of interactions  $i$  necessary to bring these nucleons down to an energy ( $\sim 5$  GeV) below which the multiplicity of pion production on a stationary target is no longer roughly constant (up to logarithmic corrections), but is suppressed by threshold effects. The argument of the previous paragraph now yields  $i \sim 4$  (6) for  $\gamma_{\text{in}} = 3 \times 10^3$  ( $10^4$ ). One may be concerned with the fact that, if the CB contains more interaction lengths than the SNS's target funnel, the last of the CB's protons to interact with the pancake (which is by then moving in the CB's direction) may only suffer collisions at a centre-of-mass energy insufficient to produce pions. To dissipate this concern, consider the very last nucleon of the CB to suffer a collision with the ensemble of the CB plus the swept-up mass, and go back to the system in which the SN is at rest. In that system, the incoming nucleon and its target have Lorentz factors  $\gamma_{\text{in}}$  and  $\gamma_{\text{out}}$ , respectively, which brings us back to the argument in the previous paragraph.

Another concern is that, if nucleons suffer only a few interactions with a large centre-of-mass energy, the earlier estimate that 2/3 of the CB's energy is lost to neutrinos may be grossly incorrect. But after  $i$  interactions the fraction of the original energy of the CB's nucleons that has been invested in pion-production is  $\alpha \simeq 1 - f^i$ , two thirds of which ends up in neutrinos. For  $i = 3$  (6),  $\alpha \sim 66\%$  ( $\sim 88\%$ ), so that Eq.(16) is a fair approximation.

Given the previous arguments, we shall estimate the neutrino flux as that produced by a nucleon beam, containing as many nucleons as the incoming CB, moving with a Lorentz factor  $\gamma_{\text{in}}$ , and interacting *thrice* on a nucleon or nuclear target. Because of “Feynman scaling”, as we shall see, it does not matter whether the target nucleons are at rest or receding with a Lorentz factor  $\gamma_{\text{out}}$ . It follows from the above discussion that this estimate of the neutrino flux is an underestimate. However, in practice the incurred error is small, because the charged pions produced in  $i \geq 4$  interactions have a relatively low energy. Since the detection efficiency of their decay neutrinos is weighted, as we shall see, by two powers of energy, the low-energy tail of the neutrino spectrum is immaterial.

## 6.2 The origin of EGRs

The SNS is only transparent to  $\gamma$ -rays in its outer layer, some  $X_{\text{EGR}} = 70 \text{ g cm}^{-2}$  deep, Eq.(10). That figure also corresponds to roughly two high-energy nucleon–nucleon interaction lengths, see Eq.(21). The shell is many interaction lengths thick, so that by the time the CB reaches the shell’s  $\gamma$ -ray transparent outer layer, it is already moving with  $\gamma \simeq \gamma_{\text{out}}$ . At that point the CB has reached a radius:

$$\tilde{R}_{\text{CB}} \sim (x_{\text{EGR}}^{\text{tp}} - R_{\text{s}}) \frac{\beta_{\text{out}}}{\gamma_{\text{out}}}. \quad (31)$$

For  $\beta_{\text{out}} = 1/\sqrt{3}$ ,  $\gamma_{\text{out}} = 10^3$  and the largest of the  $x_{\text{EGR}}^{\text{tp}}$  in Eq.(12),  $\tilde{R}_{\text{CB}} \sim 8.8 \times 10^{11} \text{ cm}$ . With this radius and the reference mass of Eq.(4) the CB’s grammage is  $M_{\text{CB}}/(\pi \tilde{R}_{\text{CB}}^2) \sim 1500 \text{ g cm}^{-2}$ , which is larger than that of the transparent outskirts of the shell,  $X_{\text{EGR}}$ . We shall therefore compute the EGR flux as that originating from the  $\pi^0$ ’s made by the front of the CB as it interacts with *all* the nucleons in the shell’s transparent outer layer<sup>5</sup>. This total number, computed in the same way as  $N_{\text{p}}^{\text{GRB}}$  in Eq.(27), is:

$$N_{\text{p}}^{\text{EGR}} \approx \pi \tilde{R}_{\text{CB}}^2 \frac{X_{\text{EGR}}}{m_{\text{p}}}, \quad (32)$$

whose numerical value is:

$$N_{\text{p}}^{\text{EGR}} \simeq (1.4 \times 10^{49}) \left[ \frac{x_{\text{EGR}}^{\text{tp}} - R_{\text{S}}}{2.2 R_{\text{S}}} \right]^2 \left[ \frac{\overline{R}_{\text{S}} \overline{\beta}_{\text{out}}}{\overline{\gamma}_{\text{out}}} \right]^2, \quad (33)$$

where the values of  $x_{\text{EGR}}^{\text{tp}}$  for various shell density indices  $n$  are those of Eq.(12) and we have not made explicit the weak dependence on  $(R_{\text{S}}^2/M_{\text{S}})$  to the power  $1/(n-1)$ .

The total energy of the EGR pulse generated by a CB, as seen by a local observer at rest in the SN system, is:

$$E_{\text{EGR}} \approx \frac{1}{3} \pi \tilde{R}_{\text{CB}}^2 X_{\text{EGR}} c^2 \gamma_{\text{out}}. \quad (34)$$

To study the spectrum and angular collimation of the EGR flux, as seen by a cosmologically distant observer, we must recall the details of pion production and decay.

## 6.3 Pion production in nucleon–nucleon collisions

The CB’s baryon number, as it crosses the SNS, resides in protons or nuclei that are been broken into their constituents by relativistic collisions. The same is the case

---

<sup>5</sup>We neglect the reinteractions with the shell’s nucleons that have already been struck one or more times and set into forward motion, thereby slightly underestimating the EGR flux.



for the funnel in the SNS that is swept up by the CB. At TeV energies, the nucleon–nucleon, nucleon–nucleus or nucleus–nucleus processes have different cross sections, but the properties of the produced pions, *per colliding nucleon–nucleon pair*, are very similar, and not significantly different for protons or neutrons. Consequently, we can use for our considerations the empirical information on pion (and kaon) production in proton–proton collisions.

Bailly et al. [37] reported on a study of inclusive charged pion production in the collisions of protons of energy 360 GeV on a hydrogen target (c.m.s. energy  $\sqrt{s} \simeq 26$  GeV), as a function of “Feynman  $x$ ”:

$$x \equiv \frac{2 E_{\pi}^{\text{cms}}}{\sqrt{s}}. \quad (35)$$

The result, roughly the same within errors for  $\pi^+$  and  $\pi^-$  is:

$$F_{\pi}(x) \equiv \frac{1}{\sigma_{\text{pp}}^{\text{TOT}}} \int dp_{\text{T}}^2 \frac{d\sigma^{\pi}}{dp_{\text{T}}^2 dx} \simeq 0.2 \frac{\pi}{x} (1-x)^{3.6}, \quad (36)$$

where  $p_{\text{T}}$  is the pion transverse momentum. Given the approximate isospin independence of the interactions, the above result should also apply to the inclusive  $\pi^0$  production. The hypothesis of Feynman scaling, satisfied up to small logarithmic corrections, is that Eq.(36) is independent of energy.

The  $x$  and  $p_{\text{T}}^2$  dependences are observed to factorize to a good approximation, and the  $d\sigma^{\pi}/dp_{\text{T}}^2$  distribution is roughly exponential, with average

$$\bar{p}_{\text{T}}^{\pi} \sim 320 \text{ MeV}. \quad (37)$$

The most precise data on transverse-momentum distributions at the relevant c.m.s. energies were collected for  $\pi^0$  production in pp interactions at the ISR collider [38]; the measured single-photon yield resulted in  $\bar{p}_{\text{T}}^{\gamma} \sim 160$  MeV, whence the result we adopt for neutral or charged pions ( $p_{\text{T}}^{\pi} \simeq 2 p_{\text{T}}^{\gamma}$ ). The double differential cross section for inclusive  $\pi$  production is therefore of the form:

$$\begin{aligned} \frac{1}{\sigma_{\text{pp}}^{\text{TOT}}} \frac{d\sigma^{\pi}}{dp_{\text{T}}^2 dx} &\simeq F_{\pi}(x) G_{\pi}(p_{\text{T}}), \\ G_{\pi}(p_{\text{T}}) &\simeq \frac{1}{2 \bar{p}_{\text{T}}^2} e^{-p_{\text{T}}/\bar{p}_{\text{T}}}, \end{aligned} \quad (38)$$

with  $F_{\pi}(x)$  as in Eq.(36) and  $\bar{p}_{\text{T}}$  as in Eq.(37). For ultrarelativistic reaction products, Eq.(38) is invariant under longitudinal Lorentz boosts, so that, with  $x \simeq E_{\pi}^{\text{lab}}/E_{\text{p}}^{\text{lab}}$ , it can be used for proton interactions on a stationary target. We shall use it for incident  $E_{\text{p}}$  up to a few TeV.

## 7 The flux of EGRs

To compute the spectrum of outgoing photons *per nucleon–nucleon collision*, we must convolute Eq.(38) with the distribution of  $\pi^0 \rightarrow \gamma\gamma$  decay. For ultrarelativistic pions, the distribution of fractional photon energies ( $w \equiv E_\gamma/E_\pi$ ) is flat and limited by  $0 < w < 1$ . The  $\gamma$  distribution in  $y \equiv E_\gamma/E_p$ , produced by the decay of pions distributed as in Eq.(36), is:

$$F_\gamma(y) = 2 \int_0^1 F_\pi(x) \frac{dx}{x} \int_0^1 dw \delta\left(w - \frac{y}{x}\right), \quad (39)$$

where the prefactor is for the two  $\gamma$ 's per  $\pi^0$  decay. To a few per cent accuracy, the result of the convolution can be fitted<sup>6</sup> by:

$$F_\gamma(y) \simeq A_\gamma \frac{1}{y} e^{-b_\gamma y} \quad (40)$$

$$A_\gamma \simeq 1.1, \quad b_\gamma \simeq 8. \quad (41)$$

The  $\gamma$ -production double differential cross-section in  $y$  and  $p_T^\gamma$  is of the same form as Eq.(38), with a longitudinal factor  $F_\gamma(y)$  and a transverse factor with  $\bar{p}_T^\gamma \sim 160$  MeV. Let  $E_\gamma$  be the energy of a photon as it reaches the Earth, cosmologically redshifted by a factor  $1+z$ , and let  $E_p \simeq m_p c^2 \gamma_{\text{out}}$  be the energy of the CB's nucleons, in the local rest system of their SN progenitor, as they reach the outer part of the SNS. For the small angles  $\theta$  at which the  $\gamma$ -rays are forward-collimated by the relativistic motion of the parent  $\pi^0$ 's, the photon-number distribution in  $x_\gamma = E_\gamma/E_p$  and  $\cos\theta$ , per single nucleon–nucleon collision, is:

$$\begin{aligned} \frac{dn_\gamma}{dx_\gamma d\cos\theta} &\simeq B_\gamma (1+z)^2 x_\gamma e^{-c_\gamma x_\gamma} \\ B_\gamma &\simeq A_\gamma \left[ \frac{m_p \gamma_{\text{out}}}{\bar{p}_T^\gamma} \right]^2 \simeq (3.76 \times 10^7) \left[ \frac{\gamma_{\text{out}}}{10^3} \right]^2 \\ c_\gamma &= c_\gamma(z, \theta, \gamma_{\text{out}}) \simeq (1+z) \left[ b_\gamma + \frac{m_p \gamma_{\text{out}} \theta}{\bar{p}_T^\gamma} \right]. \end{aligned} \quad (42)$$

Let  $dn_\gamma/d\Omega$  be the total (time-integrated) number flux of EGR photons per unit solid angle about the direction  $\theta$  (relative to the CBs' direction of motion) at which they are viewed from Earth. The photon number distribution per incident CB is:

$$\begin{aligned} \frac{dn_\gamma}{dx_\gamma d\Omega} &\sim \frac{N_p^{\text{EGR}} B_\gamma}{2\pi D_L^2} (1+z)^4 f_\gamma \\ f_\gamma &\equiv f_\gamma(z, \gamma_{\text{out}}, \theta, x_\gamma) \simeq x_\gamma e^{-c_\gamma x_\gamma}, \end{aligned} \quad (43)$$

---

<sup>6</sup>An exponential fit is inadequate close to the limit  $y = 1$ , but for  $y > 1/2$  the flux is negligible.

with  $N_p^{\text{EGR}}$  given by Eq.(33). Since a typical GRB has an average of  $n_{\text{CB}} = 5$  to 10 significant pulses, the total flux of EGRs in coincidence with a GRB may be an order of magnitude above that of Eq.(43). In Fig.(3a) we show  $f_\gamma$  as a function of  $x_\gamma$  at various  $\theta$ ; for  $z = 1$  and  $\gamma_{\text{out}} = 10^3$ . The average fractional EGR energy in the spectrum of Eq.(43) is  $\bar{x}_\gamma = 2/c_\gamma$ , corresponding, at  $z = 1$  and for  $\gamma_{\text{out}} = 10^3$ , to average energies  $\bar{E}_\gamma \sim 120$  GeV for  $\theta = 0$ ,  $\bar{E}_\gamma \sim 70$  GeV for  $\theta = 1/\gamma_{\text{out}}$ , and  $\bar{E}_\gamma \sim 40$  GeV for  $\theta = 3/\gamma_{\text{out}}$ , a more probable angle of detection [12]. Except at the highest of these energies and/or at redshifts well above unity, the absorption of  $\gamma$ -rays on the infrared background —for which we have not explicitly corrected Eq.(43)— is negligible.

Roughly characterize the efficiency of a  $\gamma$ -ray detector as a step function  $\Theta(E^\gamma - E_{\text{min}}^\gamma)$ . The total flux above threshold, per incident CB, is then:

$$\begin{aligned} \frac{dn_\gamma^{\text{T}}[x_{\text{min}}^\gamma, \theta]}{d\Omega} &\sim \frac{dn_\gamma^{\text{T}}[0, 0]}{d\Omega} G_\gamma(z, \gamma_{\text{out}}, \theta, x_{\text{min}}^\gamma) \\ G_\gamma &\simeq \left[ \frac{(1+z)b_\gamma}{c_\gamma} \right]^2 (1 + c_\gamma x_{\text{min}}^\gamma) e^{-c_\gamma x_{\text{min}}^\gamma} \\ x_{\text{min}}^\gamma &\equiv \frac{E_{\text{min}}^\gamma}{m_p \gamma_{\text{out}}} \\ \frac{dn_\gamma^{\text{T}}[0, 0]}{d\Omega} &\simeq \frac{1.1 \times 10^8}{\text{km}^2} \frac{N_p^{\text{EGR}}}{1.4 \cdot 10^{49}} \bar{\gamma}_{\text{out}}^2 \left[ \frac{1+z}{2} \right]^2 \left[ \frac{D_L(1)}{D_L(z)} \right]^2, \end{aligned} \quad (44)$$

where the scaling properties of  $N_p^{\text{EGR}}$  are those of Eq.(33). In Fig.(4a) and (4b) we show  $G_\gamma$  as a function of  $x_{\text{min}}^\gamma$  at various fixed  $\theta$ , and vice versa; for  $z = 1$  and  $\gamma_{\text{out}} = 10^3$ . The very large flux  $dn_\gamma^{\text{T}}[0, 0]/d\Omega$  of Eq.(44) is seen to be significantly reduced as soon as  $\theta$  and/or  $x_{\text{min}}^\gamma$  depart from zero: the EGR flux is not as gigantic as it appears to be at first sight.

## 7.1 EGR versus GRB total energies

An observer at a cosmological distance from a GRB source, if equipped with a detector of sufficient angular coverage, would measure a total energy per CB, in the MeV-range photons of a GRB pulse, of  $E_{\text{GRB}}^z = \gamma_{\text{out}} E_{\text{pulse}}^{\text{rest}}/(1+z)$ , with  $E_{\text{pulse}}^{\text{rest}}$  given by Eq.(28). In the multi-GeV range of the EGRs, the measurement would result in  $E_{\text{EGR}}^z = E_{\text{EGR}}/(1+z)$ , with  $E^{\text{EGR}}$  given by Eq.(34). The ratio of EGR to GRB total energies is:

$$\begin{aligned} \frac{E_{\text{EGR}}^z}{E_{\text{GRB}}^z} &\simeq r \frac{X_{\text{EGR}}^2 X_p}{X_{\text{GRB}} X_T^2} \frac{1}{\gamma_{\text{out}}} \\ r &\equiv \frac{R_{\text{EGR}}^2}{R_{\text{GRB}}^2} \simeq \left[ \frac{x_{\text{EGR}}^{\text{tp}} - R_S}{x_{\text{GRB}}^{\text{tp}} - R_S} \right]^2. \end{aligned} \quad (45)$$

The factor  $1/\gamma_{\text{out}}$  may look surprising at first: the total GRB energy is  $\propto \gamma^2$ , while the EGR energy is  $\propto \gamma$ . In both cases, one factor of  $\gamma$  is associated with individual nucleon energies. But GRB photons “benefit” from the energy associated with the bulk motion of the CB, which acts as a relativistic mirror (target SNS particles at rest, if elastically and coherently back-scattered by the much heavier CB, would recoil with a Lorentz factor  $\gamma^2$ , while particles produced in individual pp collisions would carry an energy scaling as  $\gamma$ ).

Using the results of Eqs.(11) and (12) for the transparency distances, we obtain:

$$\frac{E_{\text{EGR}}^z}{E_{\text{GRB}}^z} \simeq (0.71, 0.54, 0.26) [\bar{\gamma}_{\text{out}}]^{-1} \quad \text{for } n = (8, 6, 4), \quad (46)$$

that is, the EGRs carry almost as much energy as the GRB. Since the individual EGR photons have energies of  $\mathcal{O}(100)$  GeV, as opposed to  $\mathcal{O}(1/2)$  MeV for GRB photons, the number of EGR photons is five or six orders of magnitude below that in the associated GRB.

## 8 The flux of high energy neutrinos

The calculation of the  $\nu_\mu$  flux produced in the collision of a CB with the SNS is analogous to the calculation of the photon flux. The  $\bar{\nu}_\mu$  flux gives rise to a signal of about 1/3 the size of that of the  $\nu_\mu$  flux (we neglect it, since we find it preferable to establish a lower limit to the observational prospects). The  $\nu_\mu$ 's are made in the chain reactions  $pp \rightarrow \pi + \dots$ ,  $\pi^+ \rightarrow \mu^+ \nu_\mu$ ; and  $\pi^- \rightarrow \mu^- \bar{\nu}_\mu$ , followed by  $\mu^- \rightarrow e^- \nu_\mu \bar{\nu}_e$ . We have also estimated the contribution of K production and decay, which turns out to be negligible.

### 8.1 Pion and muon decay

We have shown in section 6.1 that, in order to estimate the neutrino flux from the CB–SNS collision, it is adequate to consider an average of  $i \sim 3$  interactions of the incoming nucleons. The leading outgoing particle in these interactions has an average transverse momentum significantly smaller than that of the produced mesons: it can be neglected. The simplest way to compute  $\nu$  fluxes is to work out first the pion distributions made in three successive interactions of the incoming nucleons and then convolute the result with the pion decay distributions. The pions made in the first interaction have the distribution of Eq.(36). To compute the distribution of those made in the two successive interactions, we must make convolutions, analogous to that in Eq.(39), with the distribution of the exiting leading-nucleon longitudinal-momentum distribution. For the latter, we use the measurements of Ref. [39]. The result,  $F_\pi^{[3]}$ , of summing the pion longitudinal distributions as functions of  $x = E_\pi/E_p$

(with  $E_p$  the original incoming nucleon's energy) can be simply parametrized, to  $\sim 15\%$  accuracy, as:

$$F_\pi^{[3]}(x) \simeq [1 + 2.2(1-x)^4] F_\pi(x), \quad (47)$$

with  $F_\pi(x)$  given by Eq.(36).

In the decay in flight  $\pi^- \rightarrow \mu^- \bar{\nu}_\mu$  of pions with  $E_\pi \gg m_\pi$ , the distributions of fractional neutrino and muon energies ( $x_\nu \equiv E_\nu/E_\pi$  and  $x_\mu \equiv E_\mu/E_\pi$ ) are flat and limited by  $0 < x_\nu < x_{\max} \equiv 1 - m_\mu^2/m_\pi^2$  and  $1 - x_{\max} < x_\mu < 1$ . The  $\nu_\mu$  distribution in  $y \equiv E_\nu/E_p$ , produced by the decay of pions distributed as in Eq.(36), is given by:

$$F_\nu(y) = \int_0^1 F_\pi^{[3]}(x) \frac{dx}{x} \int_0^{x_{\max}} \frac{dx_\nu}{x_{\max}} \delta\left(x_\nu - \frac{y}{x}\right); \quad (48)$$

the muon distribution in the decay  $\pi^- \rightarrow \mu^- \bar{\nu}_\mu$  is analogous, with the proper change of integration limits. The  $\nu_\mu$  distribution in  $z \equiv E_\nu/E_\mu$  in the decay of left-handed muons is  $3z^2$  and, upon neglect of  $m_e^2/m_\mu^2$ , it extends from 0 to 1. We do not write here explicitly the double convolution, analogous to Eq.(48), involved in the calculation of the  $y$ -distribution in  $\pi \rightarrow \mu \rightarrow \nu_\mu$  decay.

The mean  $x_\nu = E_\nu/E_\pi$  in  $\pi \rightarrow \mu\nu$  decay is  $\bar{x}_\nu = x_{\max}/2 \simeq 0.19$ , while for the muon  $\bar{x}_\mu \simeq 0.81$ . The mean  $z = E_\nu/E_\mu$  in  $\pi \rightarrow \nu_\mu \dots$  decay is  $\bar{z} = 3/4$ , so that the mean  $x_\nu$  in the  $\pi \rightarrow \mu \rightarrow \nu_\mu$  decay chain is  $\bar{x}'_\nu \simeq \bar{x}_\mu \bar{z} \simeq 0.6$ . The available rest energy in  $\pi \rightarrow \mu\nu$  or  $\mu \rightarrow e\nu\nu$  decay is small relative to the mean transverse momentum of the parent pion. This implies that the mean  $\nu_\mu$  transverse momentum in the  $\pi \rightarrow \mu\nu$  chain is  $\bar{x}_\nu \bar{p}_T \simeq 60$  MeV, where we have used Eq.(37). The corresponding result for the  $\pi \rightarrow \mu \rightarrow \nu_\mu$  chain is  $\bar{x}'_\nu \bar{p}_T \simeq 190$  MeV. We shall see that the muon detection sensitivity on Earth is weighted by two powers of energy (one for the cross section, one for the muon range), so that the  $\pi \rightarrow \mu \rightarrow \nu_\mu$  process, which produces a harder  $\nu_\mu$  beam, is harder. Rather than giving results for a two-component distribution ( $\pi \rightarrow \mu\nu$  and  $\mu \rightarrow e\nu\nu$ ) we shall use a common transverse momentum:

$$\bar{p}'_T = 190 \text{ MeV} \quad (49)$$

for the overall  $\nu_\mu$  beam. This results in a small underestimate of the flux at a fixed angle.

The relative contribution of kaons to the  $\nu_\mu$  flux is suppressed with respect to that of pions for three reasons. The  $K/\pi$  relative multiplicity is  $\sim 1/5$ ; the  $K \rightarrow \mu\nu$  branching ratio is  $\sim 63\%$ ; and the available energy in the decay is not negligible in comparison with  $\bar{p}_T^K$ . All in all, the K-decay contribution to the  $\nu_\mu$  flux at fixed angle is at the few per cent level: we neglect it altogether.

The result of all this analysis is a longitudinal distribution in  $y = E_\nu/E_p$  (with  $E_p$  the incoming nucleon's energy) that can, to a few per cent accuracy, be fitted by:

$$F_\nu(y) \simeq A_\nu \frac{1}{y} e^{-b_\nu y} \quad (50)$$

$$A_\nu \simeq 3, \quad b_\nu \simeq 12. \quad (51)$$

The  $\nu_\mu$ -production double differential cross-section in  $y$  and  $p_T^\nu$ —describing the neutrino flux generated in the beam dump per incident proton—is of the same form as Eq.(38), with a longitudinal factor  $F_\nu(y)$  and a transverse factor with  $\bar{p}_T^\nu \sim 190$  MeV.

Let  $E_\nu$  be the cosmologically redshifted energy of a neutrino as it reaches the Earth, and let  $E_p \simeq m_p c^2 \gamma_{\text{in}}$  be the energy of the CB's nucleons, in the local rest system of their SN progenitor, as they enter the SNS. In analogy with Eq.(42) the  $\nu_\mu$ -number distribution in  $x_\nu = E_\nu/E_p$  and  $\cos \theta$ , per single nucleon–nucleon collision, is:

$$\begin{aligned} \frac{dn_\nu}{dx_\nu d\cos\theta} &\simeq B_\nu (1+z)^2 x_\nu e^{-c_\nu x_\nu} \\ B_\nu &\simeq A_\nu \left[ \frac{m_p \gamma_{\text{in}}}{\bar{p}_T^\nu} \right]^2 \simeq (6.0 \times 10^7) \left[ \frac{\gamma_{\text{in}}}{10^4} \right]^2 \\ c_\nu &= c_\nu(z, \theta, \gamma_{\text{in}}) \simeq (1+z) \left[ b_\nu + \frac{m_p \gamma_{\text{in}} \theta}{\bar{p}_T^\nu} \right]. \end{aligned} \quad (52)$$

Let  $dn_\nu/d\Omega$  be the time-integrated number of neutrinos per unit solid angle about the direction  $\theta$  (relative to the CBs' direction of motion) at which they are viewed from Earth. In analogy with Eq.(43), the neutrino number distribution, per incident CB, is:

$$\begin{aligned} \frac{dn_\nu}{dx_\nu d\Omega} &= \frac{N_b B_\nu}{2\pi D_L^2} (1+z)^4 f_\nu \\ f_\nu &= f_\nu(z, \gamma_{\text{in}}, \theta, x_\nu) \simeq x_\nu e^{-c_\nu x_\nu}, \end{aligned} \quad (53)$$

with  $N_b$  the total baryon number of the CB, given by Eq.(5). For a GRB with  $n_{\text{CB}}$  significant pulses, the total number of neutrinos is  $n_{\text{CB}}$  times larger than that of Eq.(53).

In Fig.(3b) we show  $f_\nu$  as a function of  $x_\nu$  at various  $\theta$ ; for  $z = 1$  and  $\gamma_{\text{in}} = 10^4$ . The average fractional  $\nu$  energy in the spectrum of Eq.(53) is  $\bar{x}_\nu = 2/c_\nu$ , corresponding, for the chosen  $z$  and  $\gamma_{\text{in}}$ , to average energies  $\bar{E}_\nu \sim 712$  GeV for  $\theta = 0$ ,  $\bar{E}_\nu \sim 315$  GeV for  $\theta = 1/10^3$ , and  $\bar{E}_\nu \sim 150$  GeV for  $\theta = 3/10^3$ .

Neutrino oscillations may reduce the flux of  $\nu_\mu$ s of Eq.(53) by as much as a factor of 2 (if they are maximal) or even 3 (if they are “bimaximal”).

## 8.2 Muon production on Earth

Muon neutrinos produced by a GRB can be detected by large-area or large-volume detectors, in temporal and directional coincidence with a GRB  $\gamma$ -ray signal. The

detection technique typically involves the “upward-going” muons, for which there is no “atmospheric” cosmic-ray background.

A flux of neutrinos traversing rock or ice interacts with target nuclei N, producing muons in the process  $\nu_\mu + N \rightarrow \mu + \dots$ . In the energy range of interest here, the inclusive muon cross-section per target nucleon is:

$$\frac{d\sigma(E_\nu, E_\mu)}{dE_\mu} \simeq \frac{\sigma_{\text{CC}}}{E_\nu} \theta(E_\nu - E_\mu); \quad \sigma_{\text{CC}} \simeq 0.8 \times 10^{-38} \text{ cm}^2 \frac{E_\nu}{\text{GeV}}. \quad (54)$$

The produced muons lose energy and “range-out” in matter before they decay. At the energies of interest here, the muon energy loss per unit distance  $x$  (in a material of average atomic number and mass  $Z$  and  $A$ ) can be approximated by:

$$-\frac{dE}{dx} \equiv R(E) \simeq \frac{\rho}{\rho_W} R_0 (1 + B E), \quad (55)$$

where  $\rho$  is the material’s density,  $\rho_W$  is  $1 \text{ g cm}^{-2}$ , and

$$R_0 \simeq 2.12 \left[ \frac{2Z}{A} \right] \frac{\text{MeV}}{\text{cm}}; \quad B \simeq 0.125 \frac{Z}{\text{TeV}}. \quad (56)$$

In ice or a typical rock material  $2Z/A \simeq 1$ , and  $Z$  is small enough for the neglect of the  $B$  term in Eq.(55), at the muon energies we shall encounter ( $E_\mu \ll 1 \text{ TeV}$ ), to be a good approximation.

At a given position  $x$  in a target material, an (approximately  $x$ -independent)  $\nu_\mu$  flux per unit area  $dN_\nu(E_\nu)/dE_\nu dA$  gives rise to a  $\mu$  flux  $dN_\mu(E_\mu, E_\nu, x)/dE_\nu dE_\nu dA$  satisfying the equation:

$$\frac{\partial}{\partial x} \left[ \frac{dN_\mu}{dE_\nu dE_\nu dA} \right] = \rho N_A \frac{d\sigma}{dE_\mu} \frac{dN_\nu}{dE_\nu dA} + \frac{dE}{dx} \frac{\partial}{\partial E_\mu} \left[ \frac{dN_\mu}{dE_\nu dE_\nu dA} \right]. \quad (57)$$

For a target thickness much larger than the muon range, an equilibrium between the produced and slowed-down muons is reached, whereby the muon flux is independent of position and the l.h.s. of Eq.(57) vanishes. Inserting Eqs.(55) and (56) into Eq.(57) and integrating, we obtain [40]:

$$\begin{aligned} \frac{dN_\mu}{dE_\mu dA} &= \int_{E_\mu} K dE_\nu \frac{dN_\nu}{dE_\nu dA} (E_\nu - E_\mu), \\ K &\simeq \rho_W N_A \frac{1}{R_0} \frac{\sigma_{\text{CC}}}{E_\nu} \simeq 2.26 \times 10^{-12} \text{ GeV}^{-2}. \end{aligned} \quad (58)$$

Define  $x_\mu = E_\mu/E_p$ : the ratio of the energy of a muon produced on Earth to the energy  $E_p = m_p c^2 \gamma_{\text{in}}$  of the CB’s nucleons, as they enter the SNS. Substitute the

neutrino flux of Eq.(53) into Eq.(58) and integrate over neutrino energies to obtain a muon flux per incident CB:

$$\begin{aligned}
\frac{dn_\mu}{dx_\mu d\Omega} &\sim K E_p^2 \int_{x_\mu} \frac{dn_\nu}{dx_\nu d\Omega} (x_\nu - x_\mu) dx_\nu \\
&= K E_p^2 \frac{N_b B_\nu}{2\pi D_L^2} (1+z)^4 f_\mu(z, \gamma_{\text{in}}, \theta, x_\nu) \\
f_\mu &= \frac{2 + c_\nu x_\mu}{c_\nu^3} e^{-c_\nu x_\mu}, \tag{59}
\end{aligned}$$

with  $B_\nu$  and  $c_\nu$  as in Eq.(52) and  $N_b$  the total baryon number of the CB, Eq.(5). In Fig.(3c) we show  $f_\mu$  as a function of  $x_\mu$  at various  $\theta$ , for  $z = 1$  and  $\gamma_{\text{in}} = 10^4$ .

Very roughly characterize the efficiency of an experiment as a step function jumping from zero to unity at  $E^\mu = E_{\text{min}}^\mu$ . The observable number of muons per CB and per unit area, obtained by integration of Eq.(59), then is:

$$\begin{aligned}
\frac{dn_\mu^T[x_{\text{min}}^\mu, \theta]}{d\Omega} &\sim \frac{dn_\mu^T[0, 0]}{d\Omega} G_\mu(z, \gamma_{\text{in}}, \theta, x_{\text{min}}^\mu) \\
G_\mu &= \left[ \frac{(1+z) b_\nu}{c_\nu} \right]^4 \left( 1 + \frac{c_\nu x_{\text{min}}^\mu}{3} \right) e^{-c_\nu x_{\text{min}}^\mu} \\
x_{\text{min}}^\mu &\equiv \frac{E_{\text{min}}^\mu}{m_p \gamma_{\text{in}}} \\
\frac{dn_\mu^T[0, 0]}{d\Omega} &\simeq \frac{3.2 \times 10^2}{\text{km}^2} \bar{E}_{\text{CB}} \left[ \frac{\gamma_{\text{in}}}{10^4} \right]^3 \left[ \frac{D_L(1)}{D_L(z)} \right]^2. \tag{60}
\end{aligned}$$

In Figs.(5a,b) we show  $G_\mu$  as a function of  $x_{\text{min}}^\mu$  at various fixed  $\theta$ , and vice versa; for  $z = 1$  and  $\gamma_{\text{in}} = 10^4$ . The relatively large flux  $dn_\mu^T[0, 0]/d\Omega$  of Eq.(60) is seen to be very significantly reduced as  $\theta$  and/or  $x_{\text{min}}^\mu$  depart from zero. Once again, for a GRB with  $n_{\text{CB}}$  significant pulses, the total number of muons is  $n_{\text{CB}}$  times larger than that of Eq.(60), and neutrino oscillations may reduce the  $\nu_\mu$  flux by a factor 2 or 3.

## 9 Angular apertures and observational prospects

Barring the case of GRB 980425 —whose exceptional properties and their interpretation within the CB model are discussed in [22]— the equivalent spherical energies of the GRBs with measured redshifts range between  $\sim 2 \times 10^{54}$  erg (GRB 990123) and  $\sim 2 \times 10^{51}$  erg (GRB 970228). The dependence of the GRB flux on the angle  $\theta$  subtended by the CB's velocity vector and the line of sight is given by Eq.(29):  $df/d\Omega \propto (1 + \theta^2 \gamma_{\text{out}}^2)^{-3}$ . This  $\theta$  dependence is the steepest parameter dependence



of the CB model, see Fig.1 of [22]. It is therefore reasonable to attribute the range of observed equivalent spherical energies to the  $\theta$  dependence, as if GRBs were otherwise approximately standard candles. The observed three orders of magnitude spread in equivalent energy then corresponds, according to Eq.(29), to a spread of viewing angles between  $\theta \approx 0$  and  $\theta \approx 3/\gamma_{\text{out}}$ . The cutoff at the upper angle reflects the sensitivity of past and current observations.

The energies of the individual GRB  $\gamma$ -rays and the GRB fluences indicate CB Lorentz factors  $\gamma_{\text{out}} \sim 10^3$ . So does an approximately 1:1 SN/GRB association. (The geometrical fraction of currently observable GRBs, for  $\theta < 3/\gamma$ , is  $\pi\theta^2/(4\pi) \approx 9/(4\gamma^2)$ . For  $\gamma = 10^3$  this fraction precisely reconciles the SN II, Ib, Ic rate in the observable universe:  $12 \pm 5 \text{ s}^{-1}$  [41] with the corresponding GRB rate of  $\sim 10^3$  per year.)

The fluxes of  $\nu$ -induced muons and of  $\gamma$ 's of GRB and EGR energies have different  $\theta$  dependences and the circumstance that GRBs are currently observed at angles up to  $\theta \sim 3/\gamma_{\text{out}} \sim 3 \times 10^{-3}$  plays an obvious role in discussing the search for EGR and  $\nu$  signals in spatial coincidence with GRBs. The discussion is summarized in Figs.(6), where we compare the angular apertures of the three fluxes. The absolute and relative normalizations in these figures are arbitrary, so that the GRB results, based on Eq.(29), depend only on  $\gamma_{\text{out}}$ , chosen to be  $10^3$ . The EGR results, based on the second of Eqs.(44), depend also on  $z$  (chosen at  $z = 1$ ) and on  $E_{\text{min}}^\gamma$ , taken here to be 50 GeV. The  $\nu$  results, also for  $z = 1$ , are based on the second of Eqs.(60); they are for  $\gamma_{\text{in}} = 10^4$  and  $E_{\text{min}}^\mu = 50 \text{ GeV}$ .

According to Figs.(6), the EGR beam, up to very large  $\theta$ , has a broader tail than the GRB beam. In practice that means that a detector with the sensitivity to observe the EGR flux of Eq.(44) should find a signal in temporal and angular coincidence with a large fraction of detected GRBs. The  $\nu_\mu$ -induced  $\mu$  beam is about an order of magnitude narrower than the GRB beam in angle, two orders of magnitude in solid angle. Consequently, a detector with a sensitivity close to that necessary to observe the  $\mu$  flux of Eq.(60) would see coincidences with only about one in a hundred intense GRB events, that is  $\sim 1\%$  of GRBs in the upper decade of observable fluences, for which  $\theta \sim 1/\gamma_{\text{out}}$ .

To ascertain the observational prospects for EGRs and  $\nu$ 's, one would have to convolute our predicted fluxes with the sensitivities of the many large-area or large-volume  $\nu$  and EGR "telescopes" currently planned, deployed or under construction. We do not have sufficiently detailed information to do so, but a coarse look at their potential indicates that testing the CB model will neither be trivial, nor out of the question. The small area of past detectors with a capability to see EGRs, such as EGRET, would preclude the observation of the flux of Eq.(44).

## 10 Timing considerations

In the cannonball model, each CB crossing the SNS generates an individual  $\gamma$ -ray pulse in a GRB light curve. The complementary statement need not be true: not every observed pulse necessarily corresponds to a single CB, since the  $\gamma$  rays generated by sufficiently close CBs may overlap. This can be seen in the two top entries in Fig.(7), which show the lightcurves of the same ensemble of CBs crossing two SNSs, which differ only in their density-profile index; in the case of the more extensive SNS ( $n = 4$ ) the various CBs blend into a single pulse.

Each CB should generate three distinct pulses: a GRB pulse, a  $\nu$  pulse and an EGR pulse. The  $\nu$  and EGR pulses are narrower in time than the GRB pulse and they precede it. Observed with neutrinos or EGRs, then, a burst has the same pulse structure as the GRB, but the pulses are shorter and are precursors of the GRB pulses. We proceed to estimate the magnitude of these effects, illustrated in Fig.(7).

For a given density distribution of the SNS, such as that in Eq.(7), it is possible, though laborious, to explicitly compute the expected time profile of the neutrino signal. This profile is sensitive to the shape of  $\rho(x)$  at all  $x$ , including the inner part of the shell, for which no empirical data are available. Consequently, we shall only give here approximate results for the width in time of the  $\nu$  signal, and for its timing relative to the onset of a GRB pulse.

Let  $x_\nu$  be the distance from the SN centre at which the shell's grammage, as in Eq.(8), is half of the total SNS grammage, that is  $x_\nu = R_s 2^{1/(n-1)}$ . The temporal half-width of the neutrino signal,  $t_\nu$ , is roughly the time it takes the CB to reach this point<sup>7</sup>. As measured by the observer, this time is given by the same expression as Eq.(25) with the substitution of  $x_{\text{GRB}}^{\text{tp}}$  by  $x_\nu$ . The ratio of durations of a single pulse in neutrinos and in GRB  $\gamma$ -rays is:

$$\frac{t_\nu}{t_{\text{GRB}}} \sim \frac{x_\nu - R_s}{x_{\text{GRB}}^{\text{tp}} - R_s}. \quad (61)$$

For SNS density indices  $n = 8, 6$  and  $4$ , this ratio is  $0.038, 0.029$  and  $0.013$ , respectively: the duration of a  $\nu$  pulse is a few per cent of that of an individual GRB pulse. Neutrinos are emitted from the moment the CB hits the SN shell, while GRB  $\gamma$  rays can only be seen if emitted from the transparent SNS outer layer. The time difference between the onset of the corresponding pulses is  $\sim t_{\text{GRB}}$ : a  $\nu$  pulse should precede its corresponding GRB pulse by approximately the width of the GRB pulse.

The discussion of the EGR pulse follows analogous lines. The ratio of EGR and GRB pulse widths is:

$$\frac{t_{\text{EGR}}}{t_{\text{GRB}}} \sim \frac{x_{\text{EGR}}^{\text{tp}} - R_s}{x_{\text{GRB}}^{\text{tp}} - R_s}, \quad (62)$$

---

<sup>7</sup>The time needed for the ‘‘last proton’’ of the CB to catch up and interact with the rest of the colliding CB is shorter than  $t_\nu$  by a factor  $\sim \beta_{\text{in}} (\gamma_{\text{out}}/\gamma_{\text{in}})^2 R_s/(x_\nu - R_s)$ .

with  $x_{\text{EGR}}^{\text{tp}}$  given by Eq.(12). For SNS density indices  $n = 8, 6$  and  $4$ , this ratio is  $0.48, 0.42$  and  $0.29$ , respectively: the duration of an EGR pulse is shorter than that of the corresponding GRB pulse by a factor 2 or 3. The time difference between the onset of the corresponding pulses is a fraction  $1 - t_{\text{EGR}}/t_{\text{GRB}}$  of the duration of the GRB pulse: an EGR pulse should precede its corresponding GRB pulse by 50 to 70% of the width of the GRB pulse.

The light curve of an EGR pulse is proportional to the SNS shell density, corrected for absorption. For the density profile of Eq.(7) and the corresponding grammage of Eq.(8):

$$\begin{aligned} \frac{dN_{\text{EGR}}}{dt} &\propto \rho_s(x[t]) \text{Exp} \left[ -\frac{X_S(x[t])}{X_{\text{EGR}}} \right] \\ x[t] &= \frac{\gamma_{\text{out}} \delta}{1+z} ct. \end{aligned} \quad (63)$$

The considerations of this section are visualized in Fig.(7), where we have drawn the light curves of a single GRB in GRB  $\gamma$ -rays, in EGRs and in neutrinos. The timing sequence of the pulses is put in by hand and their normalizations correspond to (random) values of  $\gamma_{\text{out}}$  close to  $10^3$ , see Eq.(28). The two columns of the figure correspond to  $n = 8$  and  $n = 4$ . Notice how the EGR pulses precede the GRB pulses and are narrower: the EGR has a better time “resolution”. For neutrinos, this is even more so.

## 11 Conclusions

In the CB model of GRBs, illustrated in Fig.(1), cannonballs heated by a collision with intervening material produce GRBs by thermal emission, and their electron constituency generates GRB afterglows by bremsstrahlung, synchrotron radiation and inverse Compton up-scattering of these photons and the cosmic background radiation. The material CBs hit is an excellent “beam-dump”, so that nucleon–nucleon collisions generate a very intense and collimated flux of neutrinos. Because of absorption, the emission of energetic  $\gamma$ -rays via  $\pi^0$  production and decay is much less efficient, but by no means negligible.

The  $\nu$  flux has a total energy of the order of  $10^{53}$  erg (roughly 1/3 of the total energy in a jet of CBs, augmented by the ratio  $\gamma_{\text{out}}/\gamma_{\text{in}}$ , and reduced by the redshift factor). But individual neutrinos have energies of only a few hundred GeV, as illustrated in Fig.(3), and their enormous flux will be hard to detect, even though it is collimated within an angle  $\sim 10^{-4}$ . The detection in coincidence with GRBs will be further hampered by the fact that the GRB angular distribution is broader, as shown in Fig.(6).

The EGR flux carries roughly as much energy as the GRB, that is  $E_{\text{pulse}}^{\text{rest}} \gamma_{\text{out}} \sim 10^{48}$  erg per pulse, with  $E_{\text{pulse}}^{\text{rest}}$  as in Eq.(29). The EGR beam, as shown in Fig.(6), is somewhat broader than the GRB beam, so that the search for coincidences should be fruitful. The typical energies of EGRs, as illustrated in Fig.(3), are of tens of GeVs, and the relatively high threshold energies of current large-area detectors should be a limiting issue, as in the case of neutrinos.

The pulses of the GRB  $\gamma$ -rays should be slightly preceded by narrower pulses of EGRs and by much narrower pulses of  $\nu$ 's, as illustrated in Fig.(7). The CB model, as we have seen, predicts very specific properties and relations between the GRB, EGR and  $\nu$  spectra and light curves. In this respect, as in many others, the Cannonball Model is exceptionally falsifiable.

**Acknowledgement:** This research was supported in part by the Asher Fund For Space Research and the Fund For Promotion of Research at the Technion.

## References

- [1] E. Costa et al., Nature **387** (1997) 783.
- [2] J. van Paradijs et al., Nature **386** (1997) 686.
- [3] T.J. Galama et al., Nature **395** (1998) 670.
- [4] M.R. Metzger et al., Nature **387** (1997) 878.
- [5] B. Paczynski, Astroph. J. **308** (1986) L43; J. Goodman, Astroph. J. **308** (1986) L47; J. Goodman, A. Dar and S. Nussinov, Astroph. J. **314** (1987) L7.
- [6] S.E. Woosley, Astroph. J. **405** (1993) 273; S.E. Woosley and A.I. MacFadyen, Astron. and Astroph. **138** (1999) 499; A.I. MacFadyen and S.E. Woosley, Astroph. J. **524** (1999) 168.
- [7] B. Paczynski, Astroph. J. **494** (1998) L45.
- [8] J. Alvarez-Muniz, F. Halzen and D.W. Hooper, Phys. Rev. **D62** (2000) 093015, and references therein.
- [9] N.J. Shaviv and A. Dar, Astroph. J. **447** (1995) 863.
- [10] A. Dar, Astroph. J. **500** (1998) L93.
- [11] A. Dar and R. Plaga, Astron. and Astroph. **340** (1999) 259.
- [12] A. Dar and A. De Rújula, astro-ph/0008474, and references therein.

- [13] S. Dado, A. Dar, R. Plaga and A. De Rújula, *Optical Afterglows of GRBs in the Cannonball Model*, to be published.
- [14] A. Dar, Gamma Ray Communication Network report No. 346 (1999), gcn-circ@lheawww.gsfc.nasa.gov.
- [15] D. Reichart, *Astroph. J.* **521** (1999) L111.
- [16] T.J. Galama et al., *Astroph. J.* **536** (2000) 185.
- [17] V. Sokolov et al., astro-ph/0102492, *Astron. and Astroph.*, in press.
- [18] S. Holland et al., astro-ph/0103058, *Am. Astron. Soc.* 197 (2000) 63.03.
- [19] J. Hjorth et al., *Astroph. J.* **534** (2000) L147.
- [20] K.C. Sahu et al., *Astroph. J.* **540** (2000) 74.
- [21] A.J. Castro-Tirado et al., astro-ph/0102077, submitted to *Astron. and Astroph.*
- [22] A. Dar and A. De Rújula, astro-ph/0012227.
- [23] A. Dar and A. De Rújula, astro-ph/0102115.
- [24] I.F. Mirabel and L.F. Rodriguez, *Nature* **371** (1994) 46, *Ann. Rev. Astron. and Astroph.* **37** (1999) 409, astro-ph/0007010; L.F. Rodriguez and I.F. Mirabel, *Astroph. J.* **511** (1999) 398.
- [25] G. Ghisellini et al., *Astroph. J.* **407** (1993) 65.
- [26] L. Kedziora-Chudczer et al., *Advances in Space Research* **26** (2000) 727.
- [27] B. A. Margon, *Ann. Rev. Astron. and Astroph.* **22** (1984) 507.
- [28] T. Kotani et al., *Pubs. of the Astron. Soc. of Japan* **48** (1996) 619.
- [29] A.G. Lyne and D.R. Lorimer, *Nature* **369** (1994) 127.
- [30] A. Celotti et al., *Monthly Notices of the Royal Astron. Soc.* **286** (1997) 415.
- [31] G. Ghisellini, astro-ph/0012125.
- [32] see, for instance, T. Nakamura et al., astro-ph/0007010.
- [33] see, for instance, D.E. Groom et al., *Review of Particle Physics*, *Eur. Phys. J.* **C15** (2000) 1.
- [34] R. Fusco-Fumiano et al., *Astroph. J.* **513** (1999) L21; J.S. Kaastra et al., *Astroph. J.* **519** (1999) L119.

- [35] Y. Fuzukawa et al., astro-ph/00011257
- [36] For Cas A, see, for instance, G.E. Allen et al., *Astroph. J.* **487** (1997) L97; F. Favata et al., *Astron. and Astroph.* **324** (1997) L49; L.S. The et al., *Astron. and Astroph. Supplement* **120** (1996) 357. For IC 443, see, for instance, J.W. Keohane et al., *Astroph. J.* **484** (1997) 350. For RCW 86, see G.E. Allen et al., *American Astron. Soc.* **193** (1998) 51.01.
- [37] J.L. Bailly et al., *Z. Phys.* **C35** (1987) 309.
- [38] For a review, see, for instance, G. Giacomelli, *Int. J. Mod. Phys.* **A5** (1990) 223.
- [39] D.S. Barton et al., *Phys. Rev.* **D27** (1983) 2580; A.E. Brenner et al., *Phys. Rev.* **D26** (1982) 1497.
- [40] A. De Rújula et al., *Phys. Rep.* **99** (1983) 341.
- [41] P. Madau, M. Della Valle and N. Panagia, *Month. Not. Roy. Astron. Soc.* **297** (1998) L17.

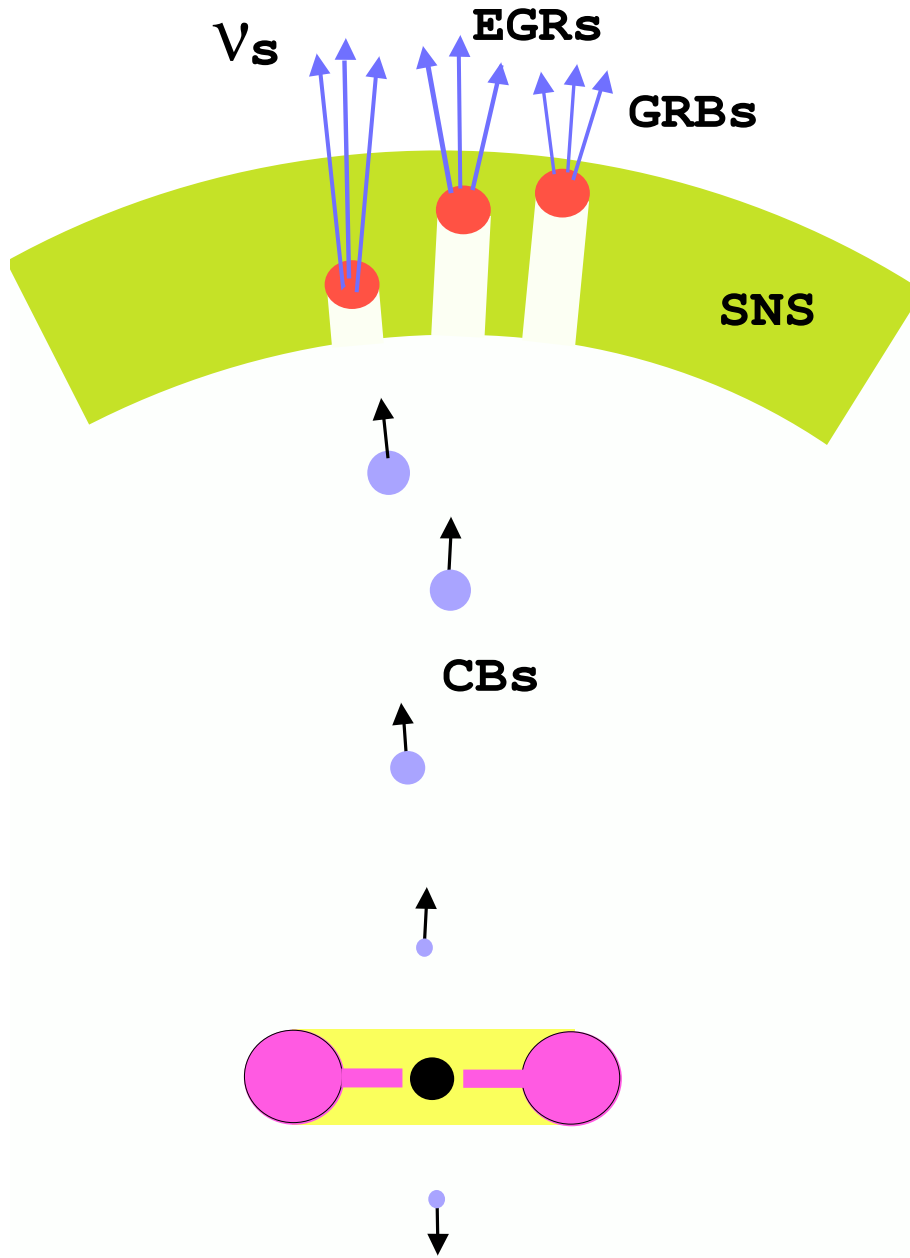


Figure 1: The CB model in a SN environment, not shown to scale. Relativistic CBs are emitted by a compact object accreting matter from a disk and/or torus. They hit a SN shell generating  $\nu$ 's, quasi-thermal radiation (the GRB) and  $\gamma$ -rays from  $\pi^0$  decay (the EGRs). The latter two exit only from the transparent outer layers of the SN shell.

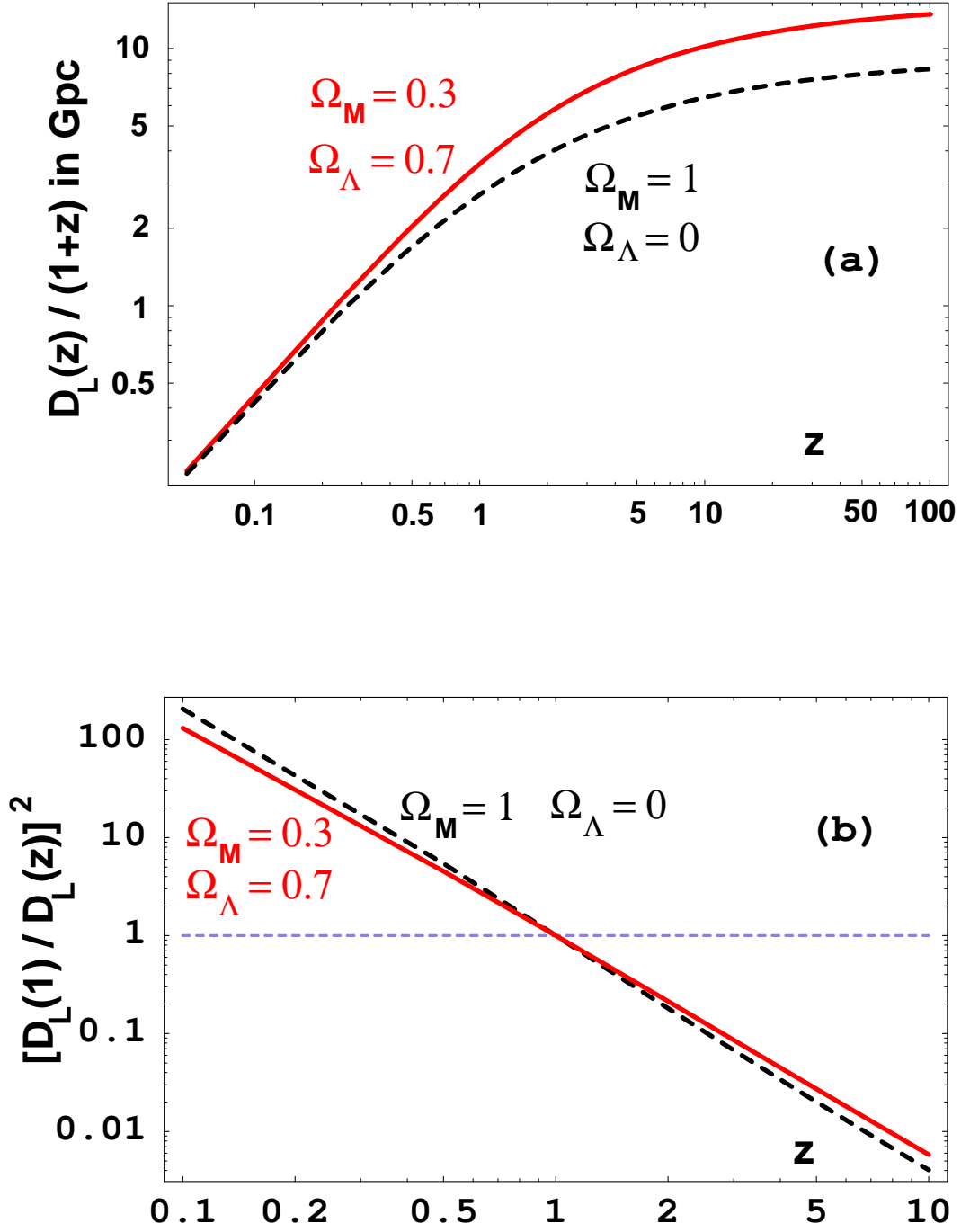


Figure 2: Luminosity distances and ratios thereof, as functions of redshift, for two  $\Omega = 1$  Friedman universes, with two choices of matter and vacuum densities.



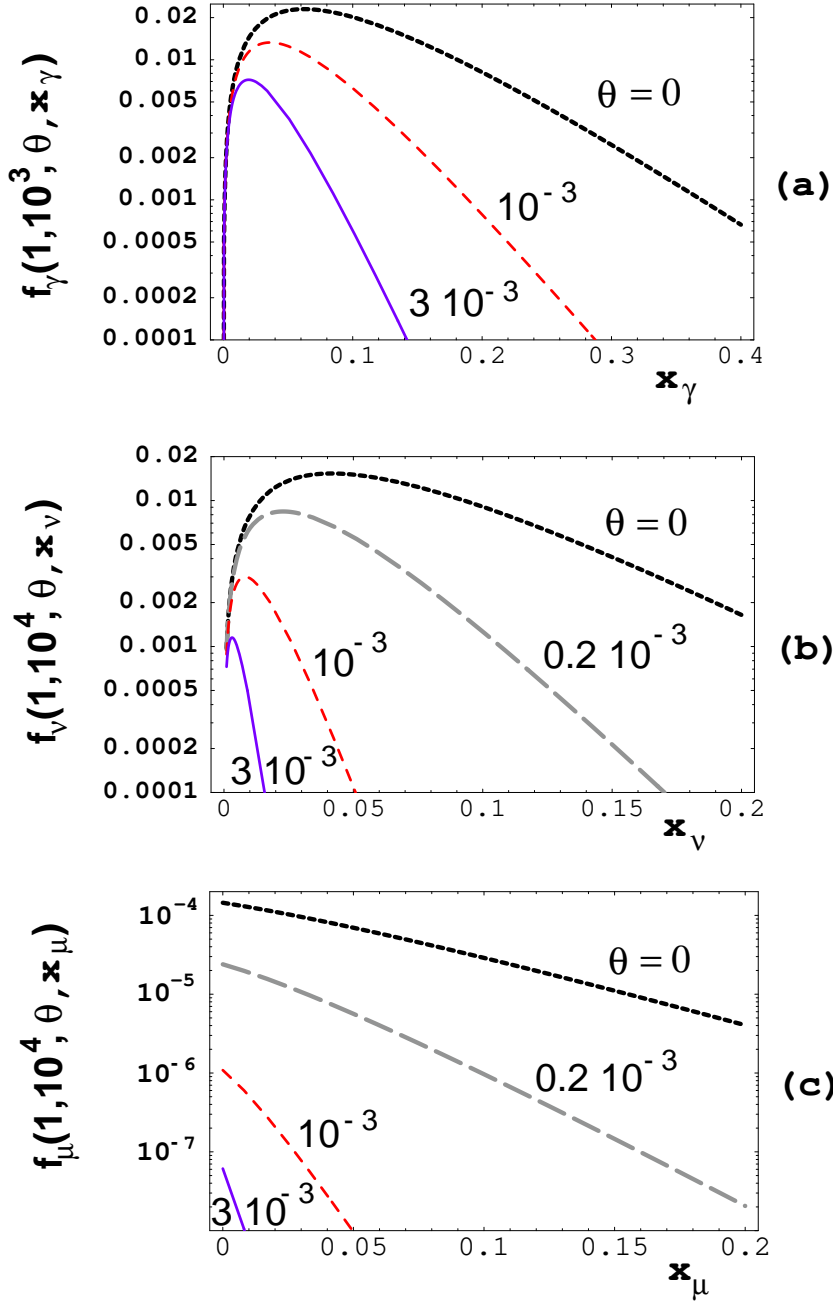


Figure 3: EGR, neutrino and muon fluxes, at various fixed observation angles  $\theta$ , as functions of the fractional momentum of the observed particle, at redshift unity. The functions  $f_\gamma(z, \gamma_{\text{out}}, \theta, \mathbf{x}_\gamma)$  of Eq.(43), for  $\gamma_{\text{out}} = 10^3$ , and  $f_{\nu,\mu}(z, \gamma_{\text{out}}, \theta, \mathbf{x}_{\nu,\mu})$  of Eqs.(53, 59), both for  $\gamma_{\text{in}} = 10^4$ , are depicted.

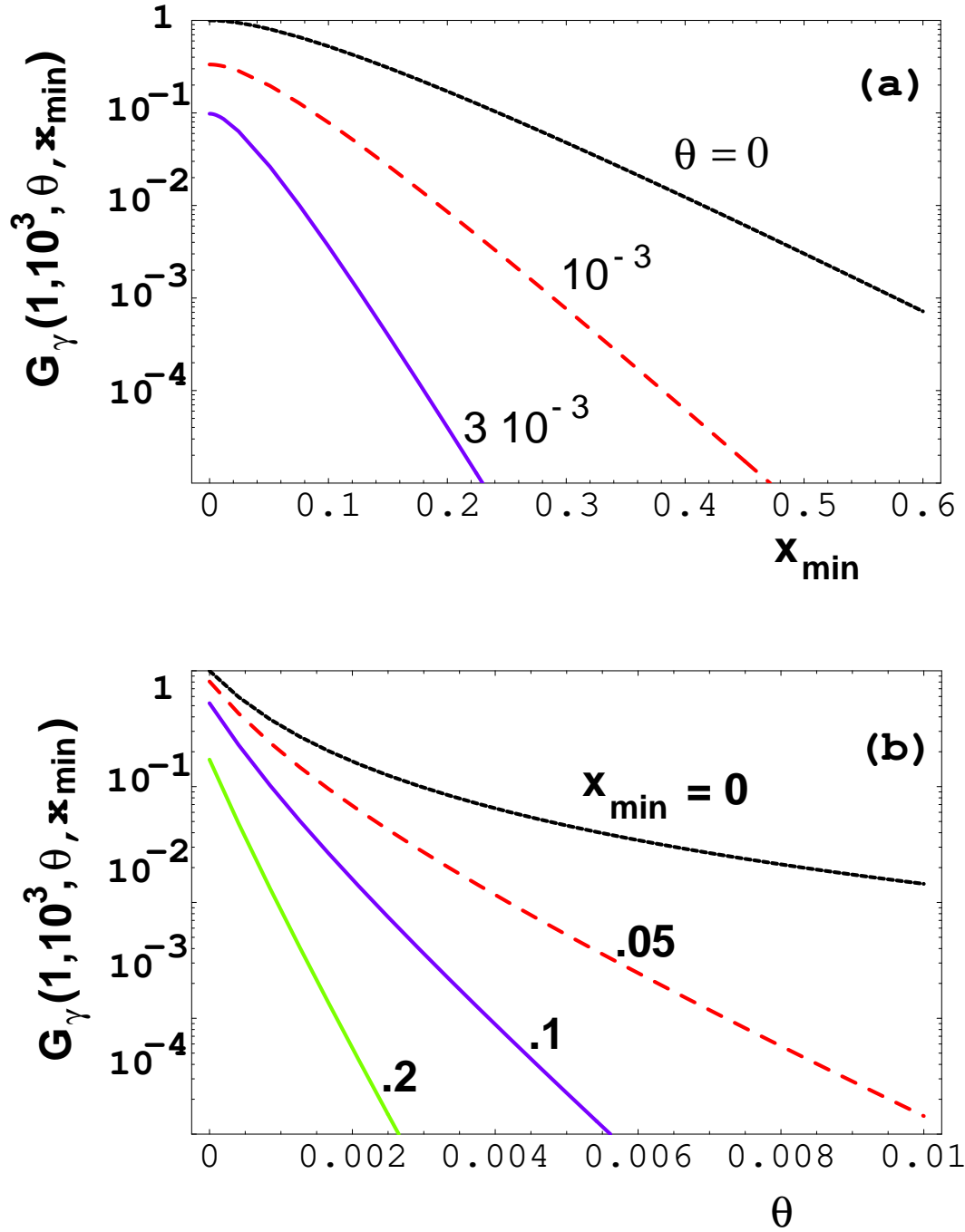


Figure 4: The function  $G_\gamma$  of Eq.(44), for  $z = 1$  and  $\gamma_{\text{out}} = 10^3$ . Top: As a function of  $x_{\min}$  at various fixed  $\theta$ . Bottom: vice versa.

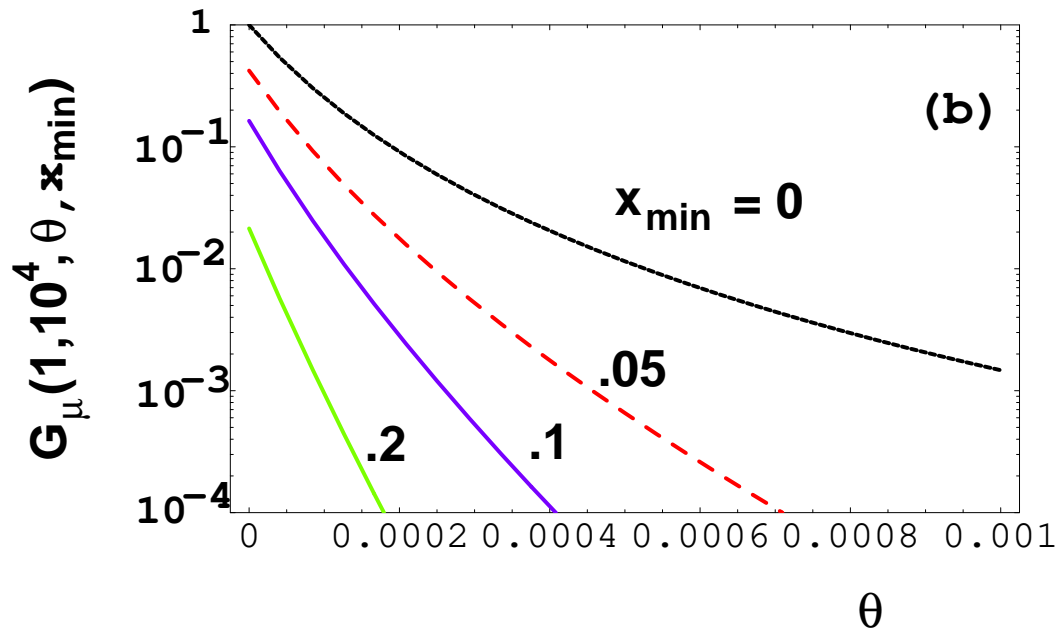
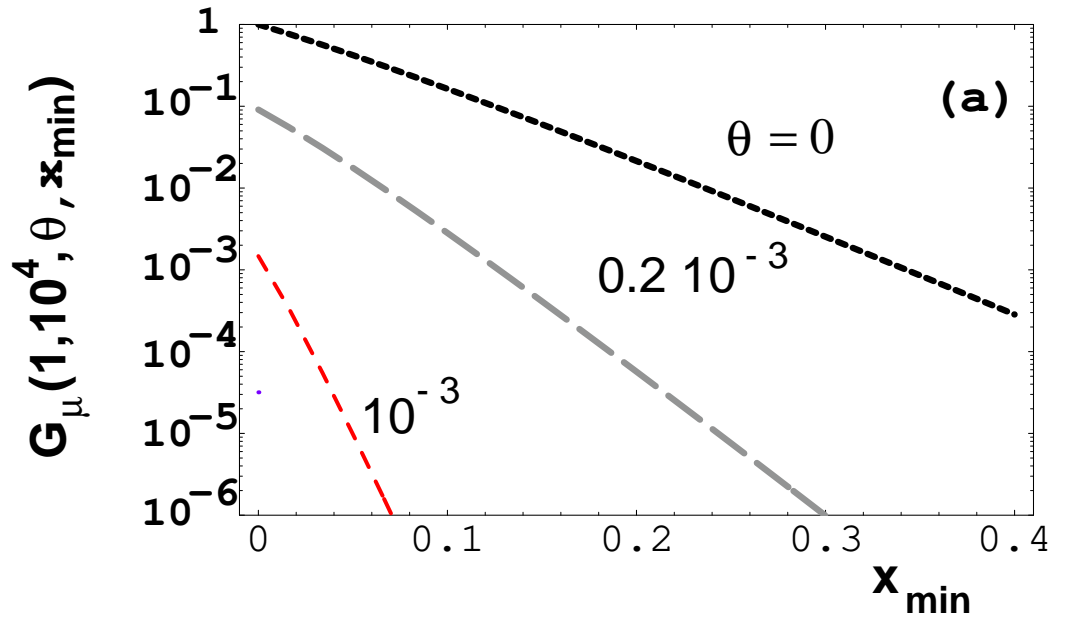


Figure 5: The function  $G_\mu$  of Eq.(60), for  $z = 1$  and  $\gamma_{\text{in}} = 10^4$ . Top: As a function of  $x_{\min}$  at various fixed  $\theta$ . Bottom: vice versa.

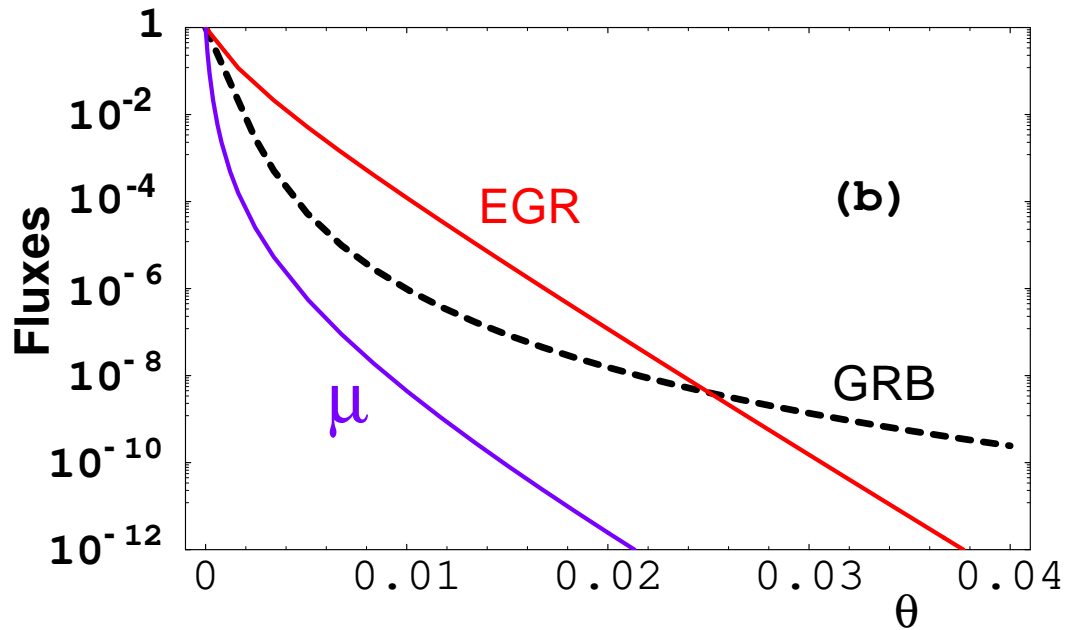
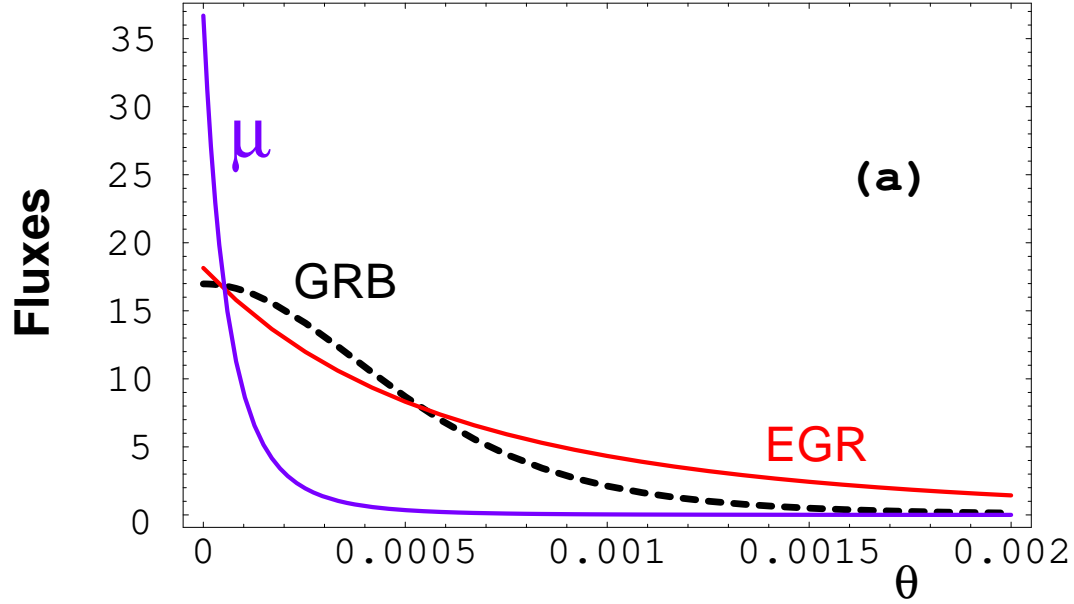


Figure 6: Comparisons of angular distributions of GRB photons, EGR photons and  $\nu$ -produced muons in water or ice. In the upper graph, the normalizations of the three curves are arbitrary. In the lower one, they are all normalized to unity at  $\theta = 0$ .

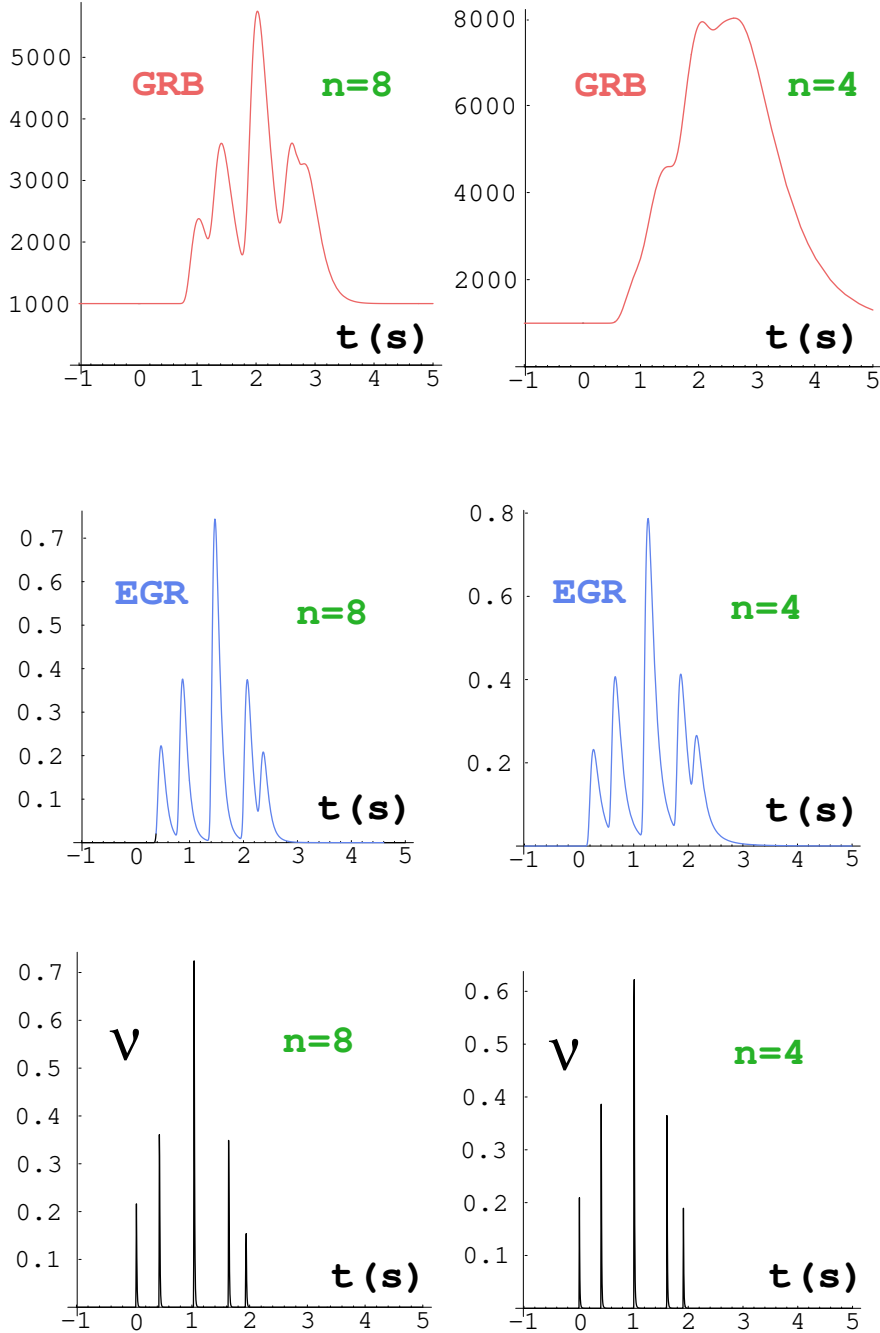


Figure 7: A “synthetic”  $\gamma$ -ray burst consisting of five CBs with  $\gamma_{\text{out}}$  within a factor of 2 of  $\gamma_{\text{out}} = 10^3$ , with other parameters at their reference values. The CBs are fired at random times in a 2.5 s interval. The two columns are for SNS density indices  $n = 8$  and 4. Top: the event seen in the 30 keV to 1 MeV GRB domain. Middle: seen in EGRs from  $\pi^0$  decay. Bottom: the neutrino signal.